Chemical Geology 425 (2016) 76–92

Contents lists available at ScienceDirect

Chemical Geology

journal homepage: www.elsevier.com/locate/chemgeo

Geochemistry of formation waters from the Wolfcamp and "Cline" shales: Insights into brine origin, reservoir connectivity, and fluid flow in the Permian Basin, USA

Mark A. Engle [a,b,*], Francisco R. Reyes [b], Matthew S. Varonka [a], William H. Orem [a], Lin Ma [b], Adam J. Ianno [b], Tiffani M. Schell [a], Pei Xu [c], Kenneth C. Carroll [d]

[a] U.S. Geological Survey, 956 National Center, Reston, VA 20192, USA
[b] Dept. of Geological Sciences, University of Texas at El Paso, 500 West University Ave., El Paso, TX 79968, USA
[c] Dept. of Civil Engineering, New Mexico State University, Las Cruces, NM 88003, USA
[d] Dept. of Plant and Environmental Sciences, New Mexico State University, Las Cruces, NM 88003, USA

ARTICLE INFO

Article history:
Received 10 September 2015
Received in revised form 26 January 2016
Accepted 28 January 2016
Available online 30 January 2016

Keywords:
Produced water
Shale oil
Tight oil
Isotope geochemistry
Permian Basin

ABSTRACT

Despite being one of the most important oil producing provinces in the United States, information on basinal hydrogeology and fluid flow in the Permian Basin of Texas and New Mexico is lacking. The source and geochemistry of brines from the basin were investigated (Ordovician- to Guadalupian-age reservoirs) by combining previously published data from conventional reservoirs with geochemical results for 39 new produced water samples, with a focus on those from shales. Salinity of the Ca–Cl-type brines in the basin generally increases with depth reaching a maximum in Devonian (median = 154 g/L) reservoirs, followed by decreases in salinity in the Silurian (median = 77 g/L) and Ordovician (median = 70 g/L) reservoirs. Isotopic data for B, O, H, and Sr and ion chemistry indicate three major types of water. Lower salinity fluids (<70 g/L) of meteoric origin in the middle and upper Permian hydrocarbon reservoirs (1.2–2.5 km depth; Guadalupian and Leonardian age) likely represent meteoric waters that infiltrated through and dissolved halite and anhydrite in the overlying evaporite layer. Saline (>100 g/L), isotopically heavy (O and H) water in Leonardian [Permian] to Pennsylvanian reservoirs (2–3.2 km depth) is evaporated, Late Permian seawater. Water from the Permian Wolfcamp and Pennsylvanian "Cline" shales, which are isotopically similar but lower in salinity and enriched in alkalis, appear to have developed their composition due to post-illitization diffusion into the shales. Samples from the "Cline" shale are further enriched with NH_4, Br, I and isotopically light B, sourced from the breakdown of marine kerogen in the unit. Lower salinity waters (<100 g/L) in Devonian and deeper reservoirs (>3 km depth), which plot near the modern local meteoric water line, are distinct from the water in overlying reservoirs. We propose that these deep meteoric waters are part of a newly identified hydrogeologic unit: the Deep Basin Meteoric Aquifer System. Chemical, isotopic, and pressure data suggest that despite over-pressuring in the Wolfcamp shale, there is little potential for vertical fluid migration to the surface environment via natural conduits.

1. Introduction

The Permian Basin of Texas and New Mexico is the most productive tight oil province in the United States, which at the time of writing this paper generates more than 2 million barrels of oil per day (U.S. Energy Information Administration, 2016). Geologic studies of the basin are numerous, given its long history in oil and gas production (Frenzel et al., 1988; Galley, 1958; Ward et al., 1986), and recent efforts have been initiated to better understand the nature of the source rocks (Cortez, 2012; Hamlin and Baumgardner, 2012; Sinclair, 2007). Despite the hundreds of geologic and petroleum resource investigations completed over the last ~80 years, studies of formation brines from the basin are sparse and primarily focused along the northern tier of the Permian Basin (Dutton, 1987; Eastoe et al., 1999; Herczeg et al., 1988; Lambert, 1992; Stein and Krumhansl, 1988), in an effort to investigate fluid movement near potential nuclear waste storage sites. The lack of investigation of formation brines in the basin is at least partly due to the long history and wide-spread use of water-flooding and CO_2 injection for enhanced recovery (Melzer, 2013), which can impact the chemistry and interpretation of formation waters (Engle and Blondes, 2014). Chemical data for produced water from recently developed mudrock and shale reservoirs in the Permian Basin are absent from published literature.

* Corresponding author at: U.S. Geological Survey, 956 National Center, Reston, VA 20192, USA.
E-mail address: engle@usgs.gov (M.A. Engle).

http://dx.doi.org/10.1016/j.chemgeo.2016.01.025

Given concerns over potential impacts from unconventional oil and gas development, ranging from toxicological effects from exposure to accidental releases of produced fluids into the environment to potential migration of injected fluids into shallow groundwater system (Vengosh et al., 2014; Vidic et al., 2013), understanding the composition of produced waters from shale reservoirs is critical (Chapman et al., 2012; Rowan et al., 2015). Moreover, investigations of reservoir pressure data (Luo et al., 1994), an important proxy for potential vertical fluid migration, are scarce and spatially limited to small areas of Delaware Basin, a sub-basin of the Permian (Fig. 1).

To provide a better hydrogeologic understanding of the Permian Basin, particularly the origin, nature, and potential flowpaths of fluids from shale reservoirs, this paper investigates the geochemistry of formation brines, with particular focus on $\delta^{18}O$, $\delta^{2}H$, $^{87}Sr/^{86}Sr$ and $\delta^{11}B$ data, from two of the most productive shale reservoirs of the basin, the Wolfcamp and "Cline" shales, as well as adjacent reservoirs. To better

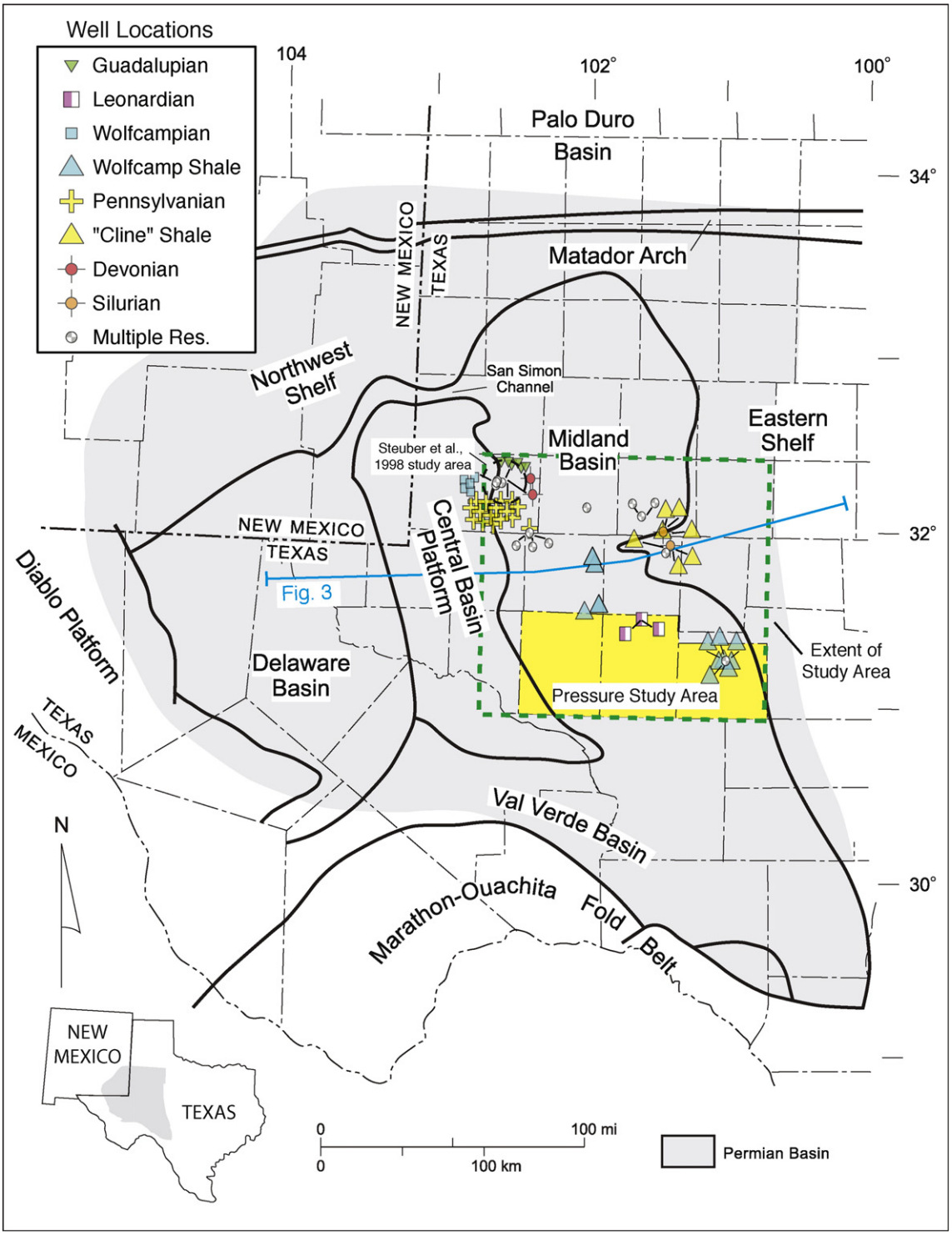

Fig. 1. Map of the Permian Basin showing major basin structures, the extent of the study area, locations of samples containing isotopic data, and the pressure study area. Well locations offset to minimize symbol overlap. Blue line shows the approximate locations of the geologic cross-section in Fig. 3. Base map modified from Dutton et al. (2005). Multiple Res. = well producing from multiple reservoirs.

represent the chemistry of natural formation waters, rather than fluids injected for fracture stimulation, the study utilizes data from wells which have been in production for months or years, such that most of the injected fluid has been removed during production or imbibed into the reservoir (Rowan et al., 2015). A subset of the samples from the Wolfcamp and "Cline" shales, collected as part of this investigation, were analyzed for organic compounds and are discussed elsewhere (Khan et al., 2016). Additional focus in this study is given to reservoir pressure data through the Paleozoic section at the center of the Midland Basin (Fig. 2) as a means to examine vertical fluid flow potential. Linked reservoir pressure and geochemical data are useful for both understanding potential for environmental impacts from development of tight oil reservoirs as well as placing constraints on basinal hydrogeology and the history of fluid flow.

2. Geology and produced waters of the Permian Basin

The present-day Permian Basin covers an area of roughly 190,000 km^2 and comprises two sub-basins, the Delaware Basin to the west and the Midland Basin to the east, separated by the Central Basin Platform (Fig. 1). It was preceded by the Tobosa Basin (Fig. 3), an interior subsidence basin in a passive margin setting which existed from the Precambrian into the early Mississippian (Frenzel et al., 1988). Lithologically, strata deposited during that period consist of shallow-water carbonates and sandstones capped with the organic-rich Woodford Shale in the Late Devonian. Collision of North America and South America, starting in the Late Mississippian and Early Pennsylvanian, led to differential subsidence behind the southwest–northeast trending Marathon–Ouachita fold belt, creating the primary features of the Permian Basin (Fig. 3), including the Delaware Basin, the Midland Basins and the Central Basin Platform (Miall, 2008). During the Pennsylvanian and Early Permian, carbonates were deposited onto the shelves (e.g., Northwest Shelf, Eastern Shelf, and Central Basin Platform) with fine-grained materials settling in the basin centers. Starting in the Late Guadalupian, there was a transition to redbed sandstone deposition and eventually evaporite formation into the Ochoan, including halite and anhydrite, on the Central Basin Platform, Northwest Shelf, Eastern Shelf and within the Midland Basin (Ward et al., 1986). Thus the sequence of Permian-age rocks in the basin, which exceeds 3000 m in areas (Fig. 4), transitions from carbonates and shale to siliciclastic sandstones and finally evaporite sequences. During the Triassic, the region shifted to a closed continental basin, receiving fluvial and lacustrine sediments, laying down a relatively thin layer of siliciclastics.

Several source rocks are present in the Permian Basin, including the Woodford, Barnett, Wolfcamp, "Cline", Dean, and Spraberry units (Fig. 2). The organic- and clay-rich layers within the Upper Pennsylvanian

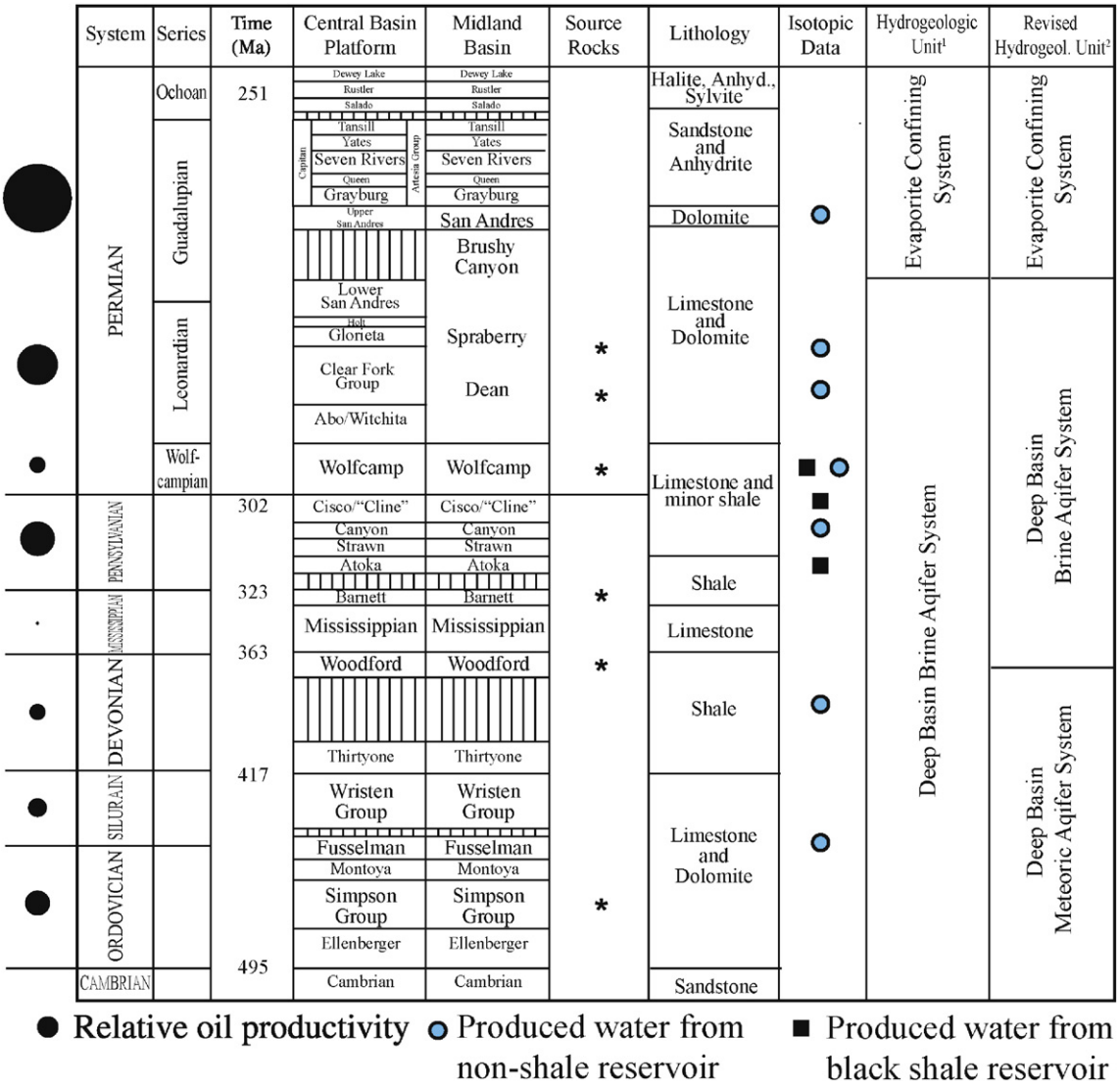

Fig. 2. Generalized stratigraphy of the Paleozoic Era of the Central Basin Platform and Midland Basin, modified from Dutton et al. (2005). Isotopic data column indicates geologic units with isotopic data for produced water samples. [1]Hydrogeologic units of Bassett and Bentley (1982). [2]Suggested revision based on findings from this paper.

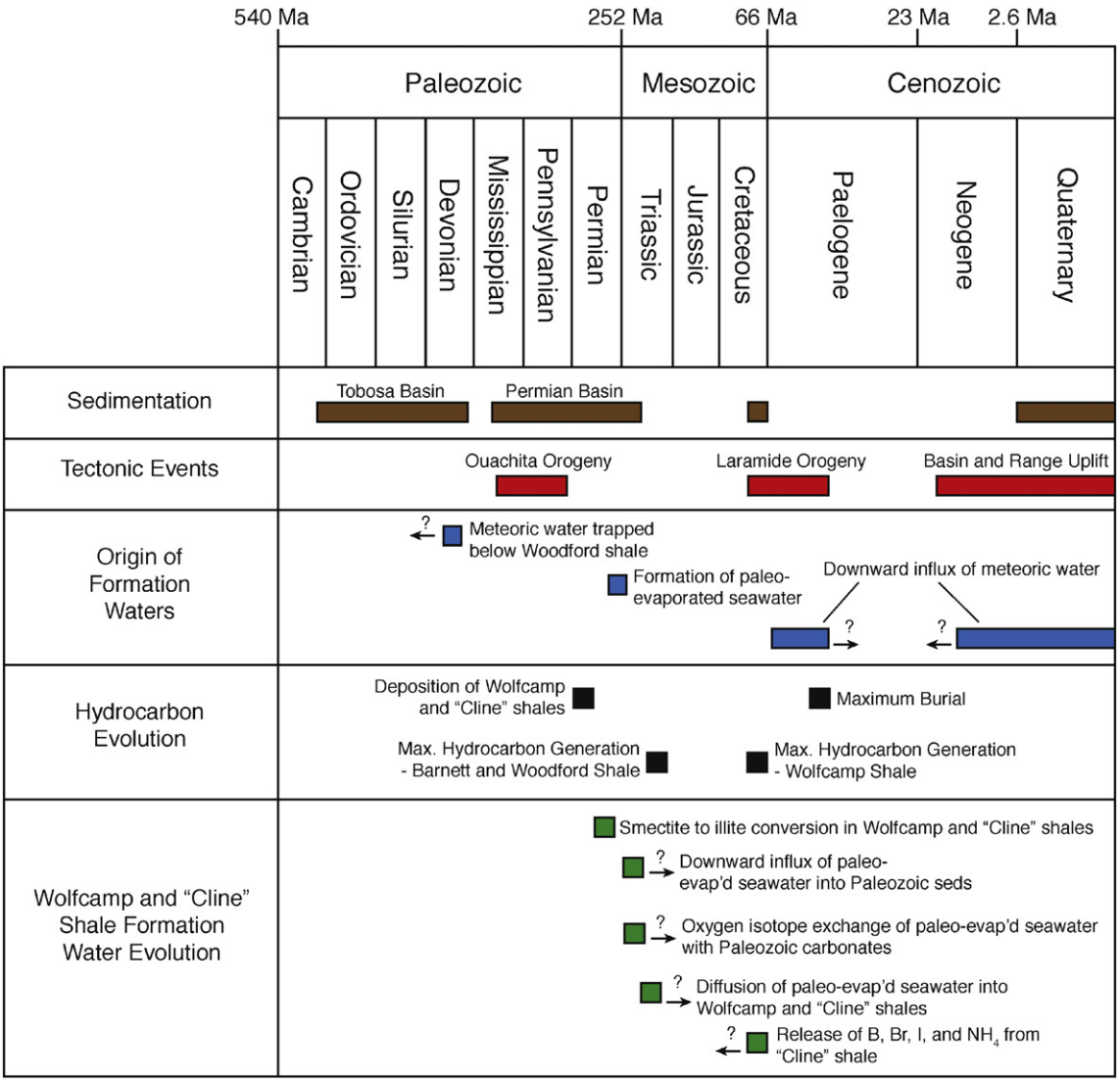

Fig. 3. Relative timing of events related to sedimentation, tectonic events, hydrogeology, water–rock interaction, and hydrocarbon evolution in the Permian Basin. Sedimentation, tectonic events, and hydrocarbon related events taken from literature cited in Section 2.

(referred to by drillers as the "Cline" shale and often divided into Upper and Lower units) and throughout the Wolfcampian rocks (Upper, Middle, and Lower Wolfcamp shale), are considered some of the most prolific source rocks of the basin (Dutton et al., 2005) and a large contributor to recent tight oil production. Wolfcampian and Pennsylvanian strata, including the Wolfcamp and "Cline" shales, thicken to the southeast toward

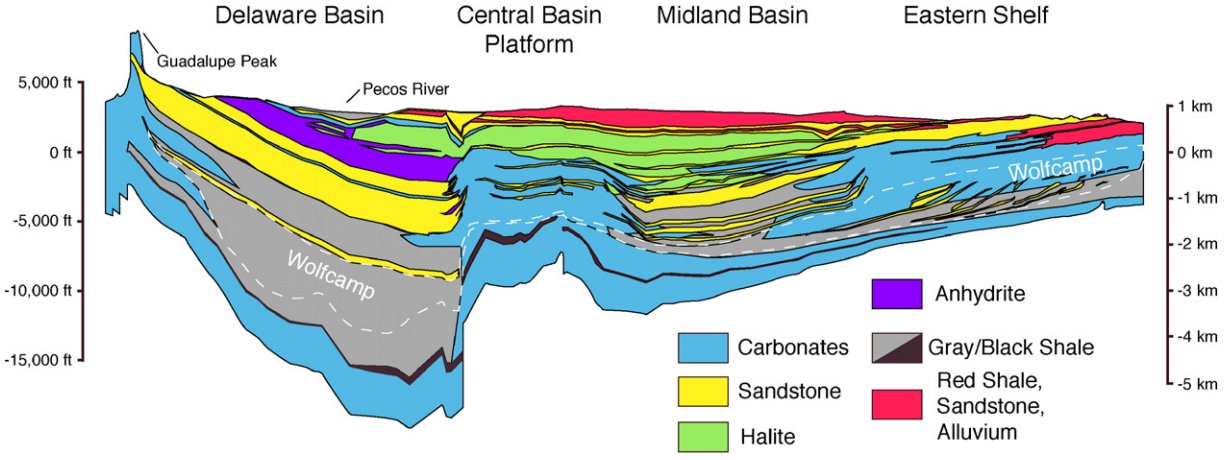

Fig. 4. Generalized geologic cross-section of the Permian Basin along the transect shown in Fig. 1. Modified from Matchus and Jones (1984).

the foredeep of the Ouachita Mountains (Hamlin and Baumgardner, 2012). Results from modeling of the Delaware Basin (Sinclair, 2007), suggest that maximum hydrocarbon generation in the deeper shales (e.g., Barnett and Woodford) occurred during the Permian, while the Wolfcamp shale achieved maximum hydrocarbon generation during the Late Cretaceous (Fig. 3). Along the edges of the Midland Basin, these units consist of platform carbonates with siliciclastics and detrital carbonate filling the basin center (Dutton et al., 2005). Lithologically, Wolfcampian and Pennsylvanian mudrocks are categorized as either calcareous mudrocks or non-calcareous mudrocks, depending on the relative contribution of carbonate minerals versus silt (Hamlin and Baumgardner, 2012). Mineralogically, the mudrocks contain quartz, feldspars, calcite, dolomite, clays (illite, smectite, chlorite and kaolinite), and less commonly pyrite and phosphate nodules (Hamlin and Baumgardner, 2012). Clays in the Wolfcampian mudrocks appear more diagenetically mature, showing substantial smectite to illite conversion (often >70% illite with R3 ordering) and higher abundances of secondary products of diagenesis (i.e., Fe-rich carbonate minerals, silica, and mixed illite–chlorite clays), than the R0 and R1 type mixed-layer clays in Pennsylvanian-age (Atokan) source rocks (Sivalingam, 1990). The availability of K in the reservoirs appears to be the primary reason that shallower Wolfcamp shale reservoirs have experienced a higher degree of diagenesis than the deeper, K-poor Pennsylvanian age shales (Sivalingam, 1990).

Previous authors studying formation brines in the area (Bassett and Bentley, 1982), primarily along the northern reaches of the Permian Basin and into the Palo Duro Basin, divided the Paleozoic strata into two hydrogeologic units (Fig. 2): 1) an Evaporite Confining System composed of halite, gypsum, and other evaporite minerals in the Ochoan and sandstone, anhydrite, and dolomite of the Guadalupian; 2) and the underlying Deep Basin Brine Aquifer System of alternating carbonates and shale, comprising all older water-bearing units. Several authors have pointed to meteoric water entering the Deep Basin Brine Aquifer System along structures in the western margins of the Permian Basin, increasing in salinity through the dissolution of evaporite minerals, and displacing older evaporated paleoseawater derived brines in piston-style flow (Barnaby et al., 2004; Bein and Dutton, 1993; Lambert, 1992; Stueber et al., 1998). However, more recent investigations of produced waters from Guadalupian reservoirs of the Delaware Basin and Central Basin Platform suggests that meteoric-derived brines are more limited in geographic extent than previously thought (Engle and Blondes, 2014).

Sinclair (2007) suggests that maximum burial of sediments in the Permian Basin occurred during the Early Eocene and was followed by uplift during the Laramide Orogeny (55–50 Ma) and Basin and Range extension (25–10 Ma). These two events removed an estimated ~1200 m and ~1100 m of sediment, respectively, from the basin. Studies from the adjacent Palo Duro Basin suggest that associated uplift and tilting created under-pressuring in portions of the Deep Basin Brine Aquifer System, due to low vertical hydraulic conductivity in the thick evaporite layers, and eastward groundwater flow (Senger et al., 1987). Although over-pressuring has been observed in some reservoirs of the Delaware Basin (Hansom and Lee, 2005; Luo et al., 1994), underpressuring in much of the Deep Basin Brine Aquifer System is inferred (Hunt, 1990). Thus, our conceptual model for present-day fluid flow in the study area is slow, but net downward flux of meteoric water from Cenozoic and Mesozoic aquifers, through the Evaporite Confining System, and into the underlying Deep Basin Brine Aquifer System, with west-to-east horizontal flow across the basin (Bein and Dutton, 1993).

3. Methods

A total of 39 (plus additional Quality Assurance/Quality Control samples) produced water samples were collected in the study area (Fig. 1) from reservoirs of Leonardian to Silurian age (Fig. 2). To better represent formation waters, rather than fluids injected for fracture stimulation, sampling was limited to wells that had been in production for more than 30 days (median value was 160 days post-production and maximum value was almost 2.5 years post-production). In addition, sampling was avoided in areas of current or historical water flooding or enhanced-oil recovery activities. With the exception of two multiple-well stock tank samples (14-TX-39B and 14-TX-40B), all samples were either collected from the production string at the pumpjack or from a separator, both of which are closed off from the atmosphere. Samples were collected in collapsible 2.5 gal carboys (Cubitainers), and processed in a manner similar to that of Kharaka et al. (1987). The carboys were inverted to allow water to settle to the bottom, below the oil and gas fractions. Water was removed through a spigot at the base of the carboy that flowed through silicone tubing to a filter assembly. The flow of water was controlled by a peristaltic pump (GeoPump2). The closed, collapsible nature of the carboy allowed for the water to be removed without exposing the samples to air. The spigot and tubing were pre-cleaned with 5% trace-metal grade nitric acid. For field parameters, a PFTE filter cartridge containing glass wool was used to remove residual oil. For ionic and organic samples, the glass wool filter was removed and replaced with a 0.45 μm capsule filter (Geotech). The carboy, silicone tubing, glass wool, and capsule filter were disposed of after each sample.

Both field parameters and laboratory measurements of brines require special methods to account for high salinity. A toroidal sensor (Omega Engineering Model CDTX-45T1), which can handle the range of high salinity samples and is not fouled by hydrocarbons or other compounds, was used to measure specific conductance (calibrated using a 200 mS/cm solution). An empirical temperature correction factor of 1.91%/°C, determined through laboratory measurements on one of the samples over a range of 10 °C to 40 °C, was applied to each field measurement. Because high salinity samples exhibit a different reference voltage than conventional pH buffers used to calibrate the instrument (Marcus, 1989), the buffers were mixed with ~85 g NaCl/L to approximate the salinity and composition of the samples. As the addition of salt to the buffers affects their pH, by changing the activity of hydrogen ions, a Pitzer-based geochemical model was used to determine the final pH of the fortified pH buffers (at 25 °C the 4.01 buffer became 3.99, the 7.00 buffer became 6.91, and the 10.0 buffer became 9.83). This method, modified from Nir et al. (2014), corrects for both differences in the activity coefficient and reference voltage in pH meters in high salinity waters. A double-junction electrode (Thermo Scientific Model ROSS 8165BNWP) was utilized to measure pH in the field, in an attempt to minimize potential of fouling of the reference electrode by sulfide. Both the pH and specific conductance units were calibrated daily and after each sampling event; no noticeable drifts were observed. Lastly, specific gravity was measured in the field using graduated hydrometers, following ASTM Method D1429-D.

Three aliquots were collected for each sample: 1) filtered and acidified (>2% distilled HNO_3) for cations, I^-, $\delta^{11}B$, and $^{87}Sr/^{86}Sr$ analyses; 2) filtered samples for anions and total dissolved solids (TDS); and 3) filtered samples in a glass, amber bottle for alkalinity, dissolved organic carbon (DOC), dissolved inorganic carbon (DIC), and isotopes of oxygen ($\delta^{18}O$) and hydrogen (δ^2H) in water. Cations and metals were analyzed via inductively coupled plasma-optical emission spectrometer (ICP-OES), iodide by ion specific electrode (ASTM D3869 — Method C), alkalinity by gran titration, and TDS by evaporation at 180 °C, all at the Department of Geological Sciences at the University of Texas of El Paso (UTEP). Anions and select cations were analyzed by ion chromatography (IC) and DIC and DOC were determined using a LICO elemental analyzer at the Energy and Environmental Lab at the U.S. Geological Survey in Reston, Virginia. Slightly better calibration data were obtained for the alkali elements from the IC method versus ICP-OES, so the IC data are reported here. Charge balances are <5% for all samples, absolute differences between field blanks (n = 4 sets) were typically <5%, and errors in the elemental reference standards (USGS M-178, M-182, T-143) were typically <10% for all elements wherein the reported values were within the calibrated range. Stable isotopes of $\delta^{18}O$ and δ^2H in water, were measured by the U.S. Geological Survey Stable Isotope Lab in Reston, Virginia. Corresponding $\delta^{18}O$ and δ^2H data were converted

from an activity basis to a concentration basis using the empirical methods of Sofer and Gat (1972, 1975).

Boron and Sr isotope measurements were carried out on a Nu Plasma multiple collector-inductively coupled plasma-mass spectrometer at the Center for Earth and Environmental Isotope Research at UTEP, following column separation in a class-100 clean room. For B, chemical separation was completed using Amberlite IRA 743 resin, following the method of Eppich et al. (2011). Data are compared to NIST 951a standard and reported in units of per mil (‰). In some samples, Fe was observed precipitating in the resin during chemical separation and was presumably transferred into the sample during elution in 2% HNO_3. However, Fe-spiked NIST 951a standard (20:1 Fe to B mass ratio) and column separated, Fe-spiked (20:1 and 5:1 Fe to B mass ratios) IAEA B-1 seawater secondary standard produced results within reported values, suggesting that Fe had no measureable impact on the analytical results. Repeated analysis of the NIST 951a standard ($n = 14$) provides an uncertainty (2s) of 1.08‰. The median value of 40.8‰ for the secondary standard, IAEA B-1, is within the range of its accepted value of 38.6 ± 3.4 ($\bar{x} \pm 2s$). For Sr, the samples were passed through Eichrom Sr-resin, dried down, and brought up in 2% HNO_3. Strontium data were corrected on-line for interferences with Kr (Konter and Storm, 2014). For the Sr isotopic measurements, the internal standard (SRM 987) exhibited an external error (2s) of 0.00016 over the 4-day analytical run, and the secondary standard (EN-1 Tridachna shell) provided a mean value of 0.70917 ± 0.00003 ($n = 8$) relative to the accepted value of 0.70917, suggesting acceptable analytical performance. Field blanks contained negligible amounts of Sr and B.

To supplement the results collected here, data for an additional 1374 produced water samples from within the study area (Fig. 1) were taken from the USGS National Produced Waters Geochemical Database, Version 2.1 (ions only; Blondes et al., 2014) and another 32 data points including results for ions, $\delta^{18}O$, $\delta^{2}H$, and $^{87}Sr/^{86}Sr$ from a study by Stueber et al. (1998) on the edge of the Central Basin Platform (Fig. 1). These additional datasets pre-date tight oil development in the Basin and are presumed to correspond to conventional, non-shale reservoirs. Like the data collected for this study, the samples from the Stueber et al. (1998) study were collected only in areas outside of current or historical water flooding or CO_2 injection. However, the impact of water flooding and CO_2 injection on the data in the USGS National Produced Waters Geochemical Database is unknown. Analysis using the database in a different portion of the Permian Basin suggested that roughly 10% of the data were impacted by water flooding (Engle and Blondes, 2014). Samples with charge imbalances >10% were excluded from analysis and are not counted in the sample totals provided here.

Ionic and elemental data are compositional, meaning that they are parts or relative amounts of some whole, and require special mathematical treatment. As noted in several papers (Engle and Blondes, 2014; Engle and Rowan, 2013, 2014), the exceptionally large range in salinities of formation waters tends to exacerbate problems associated with application of conventional data analysis to brine chemistry and make the data prone to spurious relationships. Intuitively, this is because the sum of masses or volume of the various solutes changes as a function of the water content (i.e., inverse of salinity), such that when the water content varies widely, the other solutes are artificially constrained to have a positive correlation. In some cases, the impact to the interpretation of brine geochemical data can be substantial, such as suggested mixing between end-members which is not actually occurring (Engle and Rowan, 2013). To avoid these documented issues, non-isotopic data in this paper are treated using standard compositional data analysis (CoDa) methods, which were developed specifically to overcome problems in traditional approaches (e.g., concentration vs. concentration plots). In this case, subcompositions of multivariate concentration data were converted using an isometric log-ratio (ilr) transformation prior to interpretation and plotting. The most common method for doing so is to convert D number of constituents, or parts, to $D - 1$ series of non-overlapping groups of parts known as a sequential binary partition (Egozcue and Pawlowsky-Glahn, 2005), which can be arranged to maximize geochemical interpretation (Engle and Blondes, 2014; Engle and Rowan, 2013). The corresponding ilr coordinates (z_i) are calculated using the sequential binary partition via:

$$z_i = \sqrt{\frac{r_i s_i}{r_i + s_i}} \ln \frac{(\prod x_j)^{\frac{1}{r_i}}}{(\prod x_l)^{\frac{1}{s_i}}}, \text{for } i = 1, \ldots, D-1, \tag{1}$$

where r_i and s_i are the number of parts coded with $+1$ and -1, respectively, and x_j and x_l are the constituents coded with and $+1$ and -1, respectively. For a 2-part subcomposition, say molar concentrations of Na and Cl, the resulting ilr coordinate would be:

$$z_1 = \frac{1}{\sqrt{2}} \ln \frac{[Na]}{[Cl]} \text{ or } z_1 = \frac{1}{\sqrt{2}} \ln \frac{[Cl]}{[Na]} \tag{2}$$

depending on the chosen arrangement of the sequential binary partition. Once data are transformed into ilr coordinates, they follow the standard Euclidean geometry and can be used or analyzed directly using conventional techniques. Isotopic data, for practical reasons, are not readily affected by the mathematical problems that impact concentration data and their conversion to ilr coordinates provides no substantial benefits (Blondes et al., 2015; Tolosana-Delgado et al., 2005), so they are kept in their original units.

In addition to geochemical data, formation pressure data were compiled for wells in Upton, Reagan, and Irion counties, which form the southern extent of the study area (Fig. 1). One hundred and eighteen pad initial shut-in pressure measurements for lower permeability layers in the Spraberry and Dean (both Leonardian) and from the Wolfcamp shale were taken from Friedrich and Monson (2013). Drill stem test shut-in pressure data from a proprietary database (IHS Energy)

Table 1
Geometric centers for formation water sample data from the Wolfcamp shale, non-shale Wolfcampian reservoirs, the "Cline" shale, and non-shale Pennsylvanian reservoirs within the study area. Units are percent of total solute mass.

	Wolfcamp shale	Wolfcampian	Ratio		"Cline" shale	Pennsylvanian	Ratio
Cl	6.05E−01	6.04E−01	1.00	Cl	5.75E−01	6.06E−01	0.95
Na	3.56E−01	3.13E−01	1.13	Na	3.57E−01	3.17E−01	1.13
Ca	1.77E−02	4.93E−02	0.36	Ca	2.40E−02	5.13E−02	0.47
K	4.99E−03	4.92E−03	1.01	Br	1.49E−02	2.67E−03	5.61
Br	4.87E−03	4.86E−03	1.00	Sr	1.04E−02	2.47E−03	4.19
SO_4	4.57E−03	9.03E−03	0.51	SO4	6.70E−03	6.01E−03	1.12
Sr	3.31E−03	3.55E−03	0.93	K	3.24E−03	4.00E−03	0.81
Mg	2.64E−03	8.78E−03	0.30	Mg	3.22E−03	9.87E−03	0.33
I	5.61E−04	8.60E−04	0.65	I	2.60E−03	1.71E−04	15.20
DIC	5.40E−04	3.30E−04	1.64	DIC	1.10E−03	2.83E−04	3.87
B	3.15E−04	3.21E−04	0.98	B	6.62E−04	1.81E−04	3.65
Li	2.37E−04	1.23E−04	1.94	Li	4.33E−04	9.59E−05	4.52
Si	1.06E−04	5.60E−05	1.89	Si	3.94E−04	7.17E−05	5.49

Table 2
Comparison of 1st and 3rd quartiles for water chemistry data from major tight oil and shale gas reservoirs. Bakken and Marcellus Shale data taken from the USGS National Produced Waters Geochemical Database, Version 2.1 (Blondes et al., 2014). n = number of data. Units are mg/L for all constituents except for pH (pH units).

	Wolfcamp shale — tight oil			"Cline" shale — tight oil			Bakken — tight oil			Marcellus shale — shale gas		
	Quartile 1	Quartile 3	n	Quartile 1	Quartile 3	n	Quartile 1	Quartile 3	n	Quartile 1	Quartile 3	n
pH	7.1	7.6	14	7.5	7.7	9	5.63	6.42	420	5.9	6.8	26
Alkalinity as HCO_3	412	755	14	695	1116	9	122	281	415	24.7	87.2	26
B	32.4	42.5	14	31.6	37.8	9	208	489	13	10.0	22.7	24
Ba	<20	<20	14	<20	<20	9	12.0	31.8	309	282	2605	26
Br	493	639	14	585	928	9	521	874	11	604	1126	26
Ca	1463	2762	14	647	2451	9	7142	17000	425	6055	18950	26
Cl	63052	75370	14	19750	46330	9	116399	177769	425	50475	116064	26
Fe	19.7	55.2	14	63.9	183	9	17.5	129	383	31.825	78	26
I	62.8	80.6	14	94.8	184	9	No data	No data	0	No data	No data	0
K	388	902	14	126	212	9	2598	5305	372	271	867	19
Li	25.8	28.5	10	19.5	27.3	9	7.32	57.4	16	48.0	127	25
Mg	222	384	14	84.7	329	9	667	1335.6	425	347	1675	26
Mn	<0.5	1.18	14	1.59	3.07	9	4.04	10.8	11	2.36	9.63	25
NH_4	633	1334	10	98.0	229	9	1500	2500	11	87.7	237	25
Na	38101	45095	14	12876	25207	9	57900	91700	425	26850	43742	26
Si	11.1	13.3	14	17.1	23.6	9	No data	No data	0	No data	No data	0
SO_4	363	649	14	<300	<300	9	305	760.5	422	7.3	50	25
Sr	316	421	14	293	931	9	921	1450	13	1042	3693	26
TDS	105408	123227	14	36790	79920	9	194559	292973	377	88500	199000	25
DOC	79.9	206	14	166	228	9	No data	No data	0	32.0	305	17

provided an additional 1,374 points from Guadalupian to Ordovician age reservoirs for the same three counties. Data were converted to pressure gradients to adjust for differences in reservoir depth across the study area by dividing the reservoir pressure data by the average depth of the test interval for each data point. All data with a pressure gradient less than 4.5 kPa/m were discarded as being unrealistically low.

4. Results and discussion

4.1. Geochemical characterization of Wolfcamp and "Cline" shale formation waters

Geometric centers (the geometric mean of each constituent, normalized to 100%) were used to estimate the average relative abundance of solutes by mass for produced water samples from four unique sets: 1) the Wolfcamp shale (n = 14); 2) the "Cline" shale (n = 9); 3) non-shale, Wolfcampian reservoirs; and 4) non-shale Pennsylvanian reservoirs (Table 1). By comparing the composition of produced waters from shale versus non-shale reservoirs of the similar age (Wolfcampian and Upper Pennsylvanian), it allows us to examine unique geochemical signatures and processes which affect waters found in the Permian Basin shales, where less information exists in the literature. The simple approach of determining the geometric center of each sample set is a compositional technique for approximating the multivariate barycenter of the data, while considering that the individual parts of the various solutes must sum to 100% (see Engle and Rowan [2014] for additional application of geometric centers to brine analysis). The resulting geometric centers for formation waters from Wolfcamp and "Cline" shales indicate that the solutes in sets of samples are comprised of Cl (57.5–60.6%) and Na (31.3–35.7%), with minor Ca (~5%). On average, no other constituents are present in excess of 1% by solute mass. Geometric centers for both sets also show similar relative solute abundances of Br, I, K, Mg and SO_4 (0.01% to 0.3% by solute mass) with the smallest contribution from DIC, B, Li, and Si. To allow for comparison, this analysis only includes results for elements measured/reported in all four sample sets; additional parameters of interest for these samples were examined in univariate analysis.

To gain a sense of how formation waters from the Permian Basin shale reservoirs compare to those of other shale gas and tight oil plays, univariate statistics for selected constituents in Wolfcamp and "Cline" shale produced water samples are shown with those for the Bakken (Williston Basin) tight oil and Marcellus Shale (Appalachian Basin) gas plays, taken from the USGS National Produced Waters Geochemical Database, Version 2.1 (Blondes et al., 2014). To emphasize "typical values" from formation waters, the 1st and 3rd quartiles are compared (Table 2). Use of log-ratio transformations for calculation of univariate percentile-based statistics are unnecessary because the same results are produced from the raw data (Filzmoser et al., 2009). The ranges of solute concentrations from the Wolfcamp shale samples are generally of the same order of magnitude as those from the Bakken and Marcellus Shale, but they exhibit higher pH and relatively little Ba, Ca, Mg, and Sr compared to Na. Compared to the other sets, samples of produced waters from the "Cline" shale have lower salinity (typically <80 g/L) with elevated abundances of Br and I. Data for all of these reservoirs contain elevated concentration of NH_4 (often >100 mg/L), which is unsurprising as the denitrification of organic matter in source rocks is a known source of NH_4 (Pashin et al., 2014). High ratios of alkali to alkaline earth elements and the relatively low salinity in the Permian Basin samples relative to the Bakken and Marcellus shales suggests that their origin is unique and invites further examination.

4.2. Comparison of formation water geochemistry for Wolfcamp and "Cline" shales versus adjacent formations

For a gross overview of the data, molar Na/Cl and Ca/SO_4 ratios are useful for discrimination of formation water chemistry (Hounslow, 1995). Keeping with the application of CoDa techniques, for each sample the four parts of interest (Ca, Cl, Na, and SO_4) were converted to three ilr balances using a sequential binary partition (Table 3) following the rules of Egozcue and Pawlowsky-Glahn (2005). The partition was arranged to allow for direct comparison of the molar Na/Cl and Ca/SO_4 ratios in balances 2 and 3. The resulting transformed data for these two balances are plotted in Fig. 5. Nearly all of the samples from the study area fall into the category of Ca–Cl-type brines, meaning that on an equivalence

Table 3
Sequential binary partition for the subcomposition [Ca, Cl, Na, SO_4], where + indicates that part is in the numerator of the ilr balance, − indicates that the part is in the denominator of the ilr balance, r is the number of parts in the numerator, and s is the number of parts in the denominator. Parts with neither − or + are not used in that balance.

Partition	Na	Cl	Ca	SO_4	r	s
1	+1	+1	−1	−1	2	2
2	+1	−1			1	1
3			+1	−1	1	1

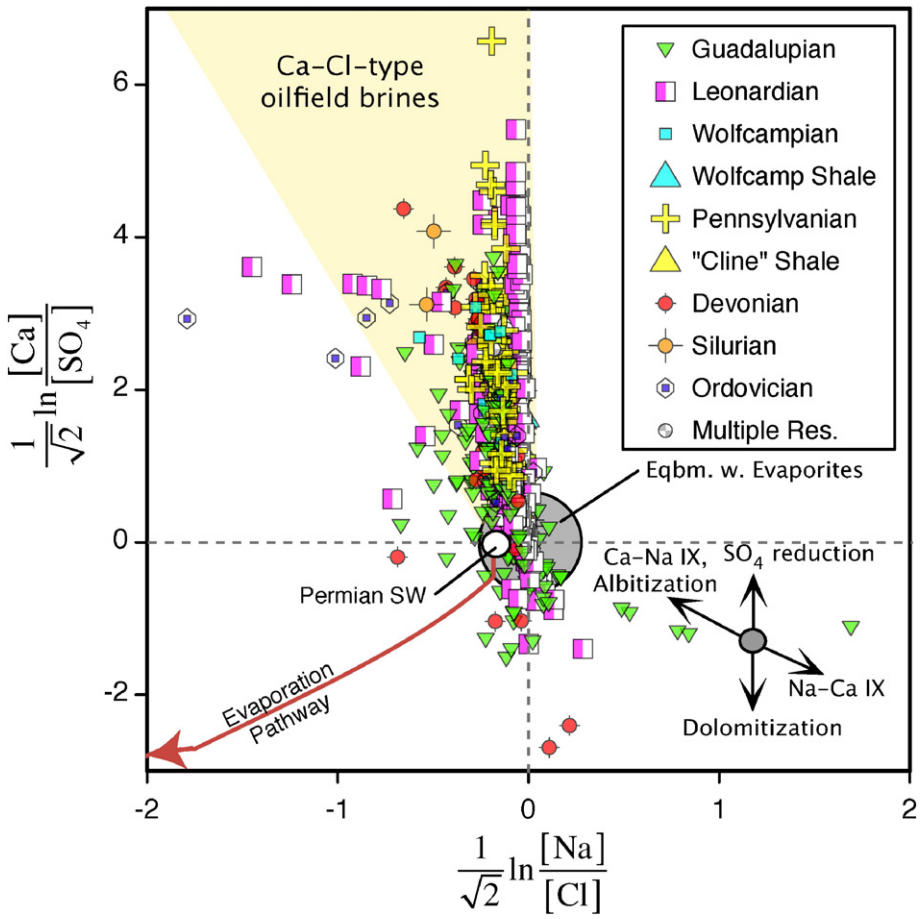

Fig. 5. Scatterplot of two isometric log-ratios for the subcomposition [Ca, Cl, Na, SO_4], using molar data. Also shown are the composition of Late Permian seawater (SW) and its modeled trajectory for evaporation (solid red line) and the approximate compositions of water in equilibrium with halite and anhydrite (gray circle). Multiple Res. = well producing from multiple reservoirs, IX = ion exchange.

basis they have more Ca than HCO_3, CO_3, and SO_4. Two potential sources of solutes, dissolution of evaporites (anhydrite and halite) and evaporated Late Permian seawater are shown on the plot, but the vast majority of data are distal to both. In fact, most of the sample data plot well above both sources on the y-axis, suggesting that SO_4 reduction has been an important process in defining the composition of formation waters from the basin. Comparison of data for formation water samples from the Wolfcamp and "Cline" shales with the adjacent non-shale reservoirs in this plot shows no obvious patterns of separation, indicating a common origin. Some of the data, particularly for samples from Guadalupian, Leonardian, and Devonian reservoirs, plot distal to the rest of the data and away from the various solute sources. These scattered data are from the USGS National Produced Waters Geochemical Database, which does include data impacted by water flooding (Engle and Blondes, 2014) and may represent mixtures of formation water with water from other sources or erroneous chemical data. Alternatively, these same compositions can be achieved through exchange of Na for Ca on clay minerals from waters in equilibrium with anhydrite and halite. Engle and Blondes (2014) previously noted that Na–Ca exchange is an important reaction in some Guadalupian-age reservoirs in the Permian Basin.

Examining the behavior of Na, Cl, and Br in saline waters has long been used to indicate the origin of salinity in brines, because Br has little affinity for halite (McCaffrey et al., 1987; Walter et al., 1990). The conventional approach is to examine either the concentrations of Cl vs. Br (or Na vs. Br) or the ratios of Na/Br vs. Cl/Br. For comparison, we show those two plots (Fig. 6) against the isometric log-ratio Na–Cl–Br graph of Engle and Rowan (2013), for the purpose of highlighting some advantages of application of compositional data analysis to brine geochemistry relative to traditional approaches. A more detailed comparison between these various plots using different datasets is provided in Engle and Rowan (2013).

The three plots (Fig. 6) show the different geochemical pathways for the evaporation of Late Permian seawater versus dissolution of Br-poor halite by paleoseawater (creation of pathways described in Engle and Blondes, 2014; Engle and Rowan, 2013) based on the assumption that halite has no affinity for Br. Plotting of Permian Basin produced water data on a Cl vs. Br concentration plot (Fig. 6A) shows that many of the data for samples from Guadalupian and some of the data from Leonardian reservoirs plot along or near the trend for halite dissolution, while those from deeper reservoirs (except for those from the Wolfcamp and "Cline" shales and the remaining Leonardian samples) generally plot along the trajectory for Late Permian seawater evaporation, prior to halite saturation. Of the remaining samples, data from the Wolfcamp shale and some of the Leonardian samples appear to plot along a mixing pathway between weakly evaporated Permian seawater and highly evaporated Permian seawater (beyond halite saturation), while those for "Cline" shale plot away for all indicated processes controlling Br and Cl.

By comparison, results using the Cl/Br vs. Na/Br plot of Walter et al. (1990) show somewhat similar results (Fig. 6B). On this type of plot, for samples to lie along the seawater evaporation curve they have to have been evaporated beyond the point of halite saturation. Therefore, results from this plot indicate that most samples which plot along the evaporation pathway are more strongly evaporated (i.e., beyond halite saturation) than suggested by the Cl vs. Br concentration plot. Moreover, on the Cl/Br vs. Na/Br diagram, data for samples for shale reservoirs plot on the far end of the seawater evaporation curve, although with a lower Cl/Br molar ratio than would be expected purely from Late Permian

seawater evaporation. If the Wolfcamp shale and a portion of the Leonardian reservoirs data do represent mixing (as suggested in the Cl vs. Br concentration plot), this plot suggests brines from the "Cline" shale may be the highly evaporated end-member (which is not supported by the concentration plot or by TDS data [Fig. 7]).

Interpretation of the isometric log-ratio Na–Cl–Br plot (Fig. 6C), an application of CoDa, shows similar results to the other two plots with some important exceptions. As before, data for samples from Guadalupian, some Leonardian, and some Devonian data plot along the curvilinear pathway (where the molar Na/Cl ratio approaches 1 and abundance of Na and Cl relative to Br, increases) for halite dissolution, suggesting these are meteoric waters that derived their salinity from upper Permian evaporite minerals. On this type of plot, mixtures of highly evaporated seawater and less evaporated seawater (as suggested for the Wolfcamp shale data by the Cl vs. Br concentration plot) fall along the seawater evaporation trajectory (Engle and Rowan, 2013). So, unlike the other two plots, formation waters from the Wolfcamp shale do not appear to represent mixtures of strongly and weakly evaporated seawater. In fact, very few samples plot along the seawater evaporation pathway. Rather, data for Wolfcampian, Wolfcamp shale, Pennsylvanian, "Cline" shale, and a portion of the Leonardian reservoir samples plot off the seawater evaporation pathway. This pattern is most pronounced for "Cline" and Wolfcamp shale formation water data, which appear to show an exceptional enrichment in Br relative to Na and Cl, and enrichment of Na relative to Cl. The former suggests input from a Br source in addition to or other than evaporated seawater. Addition of external Br would produce an exaggerated degree of evaporation in the Cl/Br vs. Na/Br plot and explain why "Cline" and Wolfcamp shale sample data in this plot indicate evaporation well beyond halite dissolution, despite showing lower TDS values than the data for non-shale Pennsylvanian and Wolfcampian reservoirs (Fig. 7). In the Cl. vs. Br concentration plot, input of external Br would push samples to the right of the evaporation pathway in creating an apparent mixing pathway for the Wolfcamp shale samples that may not truly exist. Enrichment in Na relative to Cl in the ilr plot, was not identified in the other plots and is important as it suggests additional processes that controlled the relative abundance of cations (as detailed further in Section 4.3). In this case, results from the ilr Na–Cl–Br plot (Fig. 6C) produce the most internally consistent interpretations and identify processes which were not seen in the other plots. This example highlights the advantages of application of CoDa techniques to the interpretation of brine geochemical data, and is justification for their usage here. Because data from many of the samples, including those from the shale reservoirs, fall off the modeled trajectories in the ilr Na–Cl–Br plot, application of Na–Cl–Br systematics to interpret the origin of brines to Permian Basin samples needs to be used with caution. In addition to the lack of clarity due to an external source of Br (e.g., organic-matter derived halogens), previous authors suggest that recycling of halite in the nearby Palo Duro Basin was common along basin margins (Hovorka et al., 1993), which may further complicate Na–Cl–Br systematics in Permian Basin brines.

As a final means to examine geochemical differences among formation waters found in shale reservoirs and adjacent non-shale reservoirs, histograms of TDS concentrations (Fig. 7) and compositional geometric centers (Table 2) of produced water samples from different reservoirs were examined. In general, following the modes of the histograms, TDS increases as a function of reservoir age (a proxy for depth), down to the Devonian-age reservoirs (up to and exceeding 200,000 mg/L), then decreases to <150,000 mg/L in water samples from older, deeper reservoirs (Fig. 7). Some of the lower TDS values in the conventional reservoirs may be a result of the injection of shallow meteoric water during water flooding. Formation waters from the shale units are typically 75,000–100,000 mg/L less saline than water from the adjacent, non-shale reservoirs, suggesting marked differences in formation water geochemistry between shale and non-shale reservoirs of similar age. For the Wolfcampian-age reservoirs, relative abundances of B, Br, Cl, and K were similar between geometric centers for the shale versus non-shale reservoirs (Table 2). However, the produced water samples from the Wolfcamp shale are enriched in DIC, Li, Na and Si and depleted in Ca, I, Mg, and SO_4 compared to their relative abundances in data for Wolfcampian non-shale reservoirs. Differences based on reservoir lithology were even more pronounced in the relative abundances of constituents for "Cline" shale samples versus non-shale Pennsylvanian reservoirs; samples from the shale reservoirs are heavily enriched in Br, B, DIC, I, Li, Si, and Sr, moderately enriched in Na and SO_4, and heavily depleted in K, Ca, and Mg relative to data from the non-shale reservoir samples.

Breakdown of Type-II, marine kerogen is a known source of halogens (Br and I), NH_4, and B to formation waters (Moran, 1996; Pashin et al., 2014; Williams et al., 2001b; Worden, 1996). The associated enrichment of these constituents in formation waters from the "Cline" shale relative to those from non-shale Pennsylvanian reservoirs suggests that thermal maturation of kerogen is an important control on the composition of the produced waters from mature source rocks. Additional evidence for contribution of elements from kerogen to formation waters from the "Cline" shale comes from $\delta^{11}B$ and Cl data. Strictly following rules for CoDa, a 3-part singular binary partition for this system was created (Table 4). To simplify the associated ilr coordinates, z_1 was changed from

$$\sqrt{\frac{2}{3}}\ln\frac{\sqrt{[^{11}B][^{10}B]}}{[Cl]} \tag{3}$$

to

$$\frac{1}{\sqrt{2}}\ln\frac{[B]}{[Cl]} \tag{4}$$

and z_2 was modified from

$$\frac{1}{\sqrt{2}}\ln\frac{[^{11}B]}{[^{10}B]} \tag{5}$$

to $\delta^{11}B$ (Fig. 8). This is justified because calculated values from the simplified formulas are highly correlated with those from the original coordinates ($R^2 > 0.9999$). Correspondingly transformed data for water from Leonardian and Wolfcamp shale reservoirs plot along the approximate trajectory for seawater evaporation (Vengosh et al., 1992) with a starting point for the estimated composition of Late Permian seawater (Joachimski et al., 2005). By comparison, data for the "Cline" shale water samples show enrichment in B/Cl by up to a factor of five, and exhibit isotopically lighter values of $\delta^{11}B$. Williams et al. (2001b) showed a similar pattern in formation waters from the Gulf Coast Basin and demonstrated that thermally mature marine kerogen is an important source of isotopically light B in some reservoirs, supporting this hypothesis.

Many of the other differences, in terms of salinity and solute composition, between formation waters from the shales versus adjacent, non-shale reservoirs cannot be explained by conventional mechanisms, such as preferential expulsion of solutes during physical compaction of clays (Engelhardt and Gaida, 1963; Rosenbaum, 1976) or release of interlayer water during smectite to illite conversion (Schmidt, 1973). These are sequential mechanisms (physical compaction occurs at 0–2 km burial and smectite to illite conversion at >3 km; Bjølykke, 1998), and the clay minerals of the Wolfcamp shale and less so the "Cline" shales have been

Fig. 6. A) Scatter plot of Cl versus Br concentration data; B) scatterplot of Cl/Br vs. Na/Br molar ratios of Walter et al. (1990); C) scatterplots for the ilr transformation of the [Na, Cl, Br] subcomposition. Further details on the ilr plot are found in Engle and Rowan (2013). Modeled pathways for Late Permian seawater evaporation (solid red line) and halite dissolution by seawater (dashed red line) shown on all plots. Multiple Res. = well producing from multiple reservoirs.

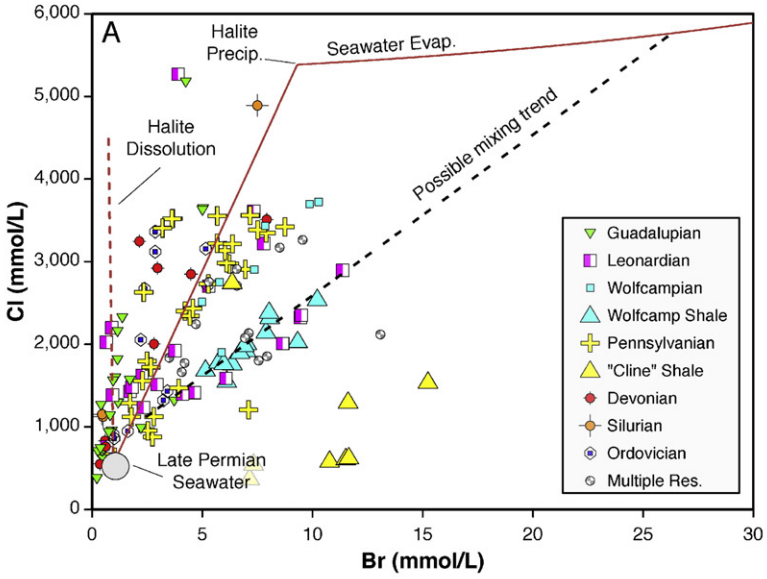
A
Halite Precip.
Seawater Evap.
Halite Dissolution
Possible mixing trend
Late Permian Seawater
Guadalupian
Leonardian
Wolfcampian
Wolfcamp Shale
Pennsylvanian
"Cline" Shale
Devonian
Silurian
Ordovician
Multiple Res.
Cl (mmol/L)
Br (mmol/L)
0
1,000
2,000
3,000
4,000
5,000
6,000
0
5
10
15
20
25
30

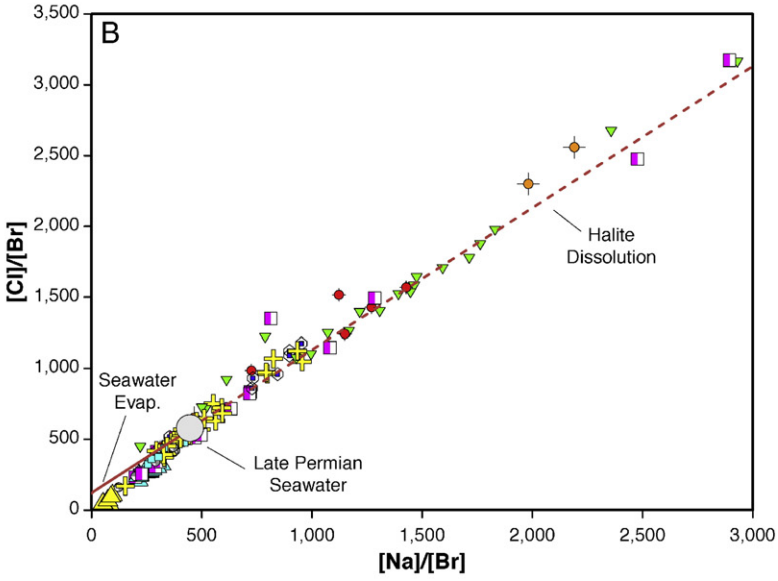
B
Halite Dissolution
Seawater Evap.
Late Permian Seawater
[Cl]/[Br]
[Na]/[Br]
0
500
1,000
1,500
2,000
2,500
3,000
3,500
0
500
1,000
1,500
2,000
2,500
3,000

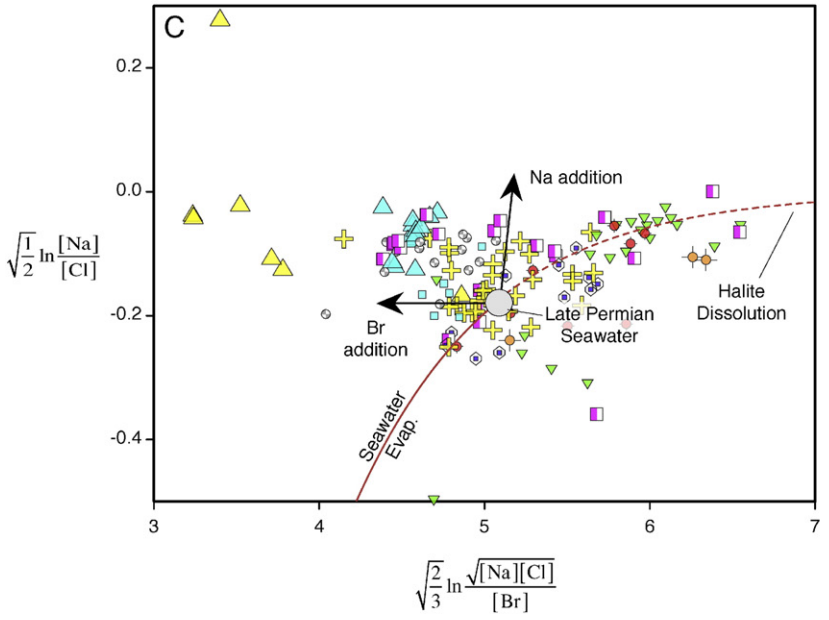
C
Na addition
Br addition
Late Permian Seawater
Halite Dissolution
Seawater Evap.
$\sqrt{\frac{1}{2}}\ln\frac{[Na]}{[Cl]}$
$\sqrt{\frac{2}{3}}\ln\frac{\sqrt{[Na][Cl]}}{[Br]}$
0.2
0.0
-0.2
-0.4
3
4
5
6
7

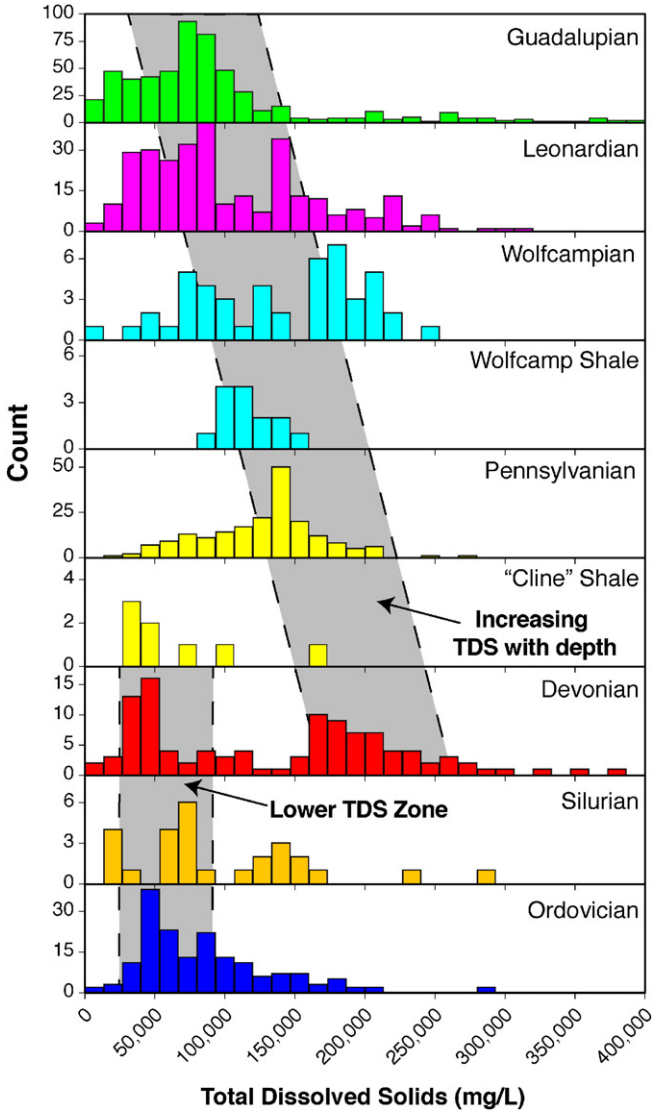

Fig. 7. Histograms of total dissolved solid (TDS) concentrations in produced water samples from Guadalupian to Ordovician reservoirs. Gray windows show trends in salinity with reservoir age drawn using modes of the histograms.

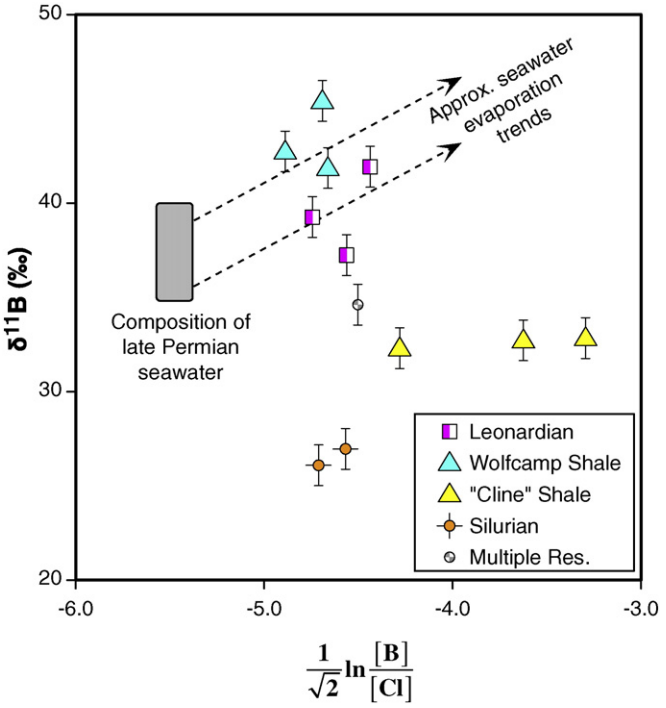

Fig. 8. Scatterplot of $\delta^{11}B$ versus ilr transformed molar B:Cl ratios. Also shown are the composition of Late Permian seawater from Joachimski et al. (2005) and the approximate trajectory for seawater evaporation calculated from data provided in Vengosh et al. (1992). Error bars in $\delta^{11}B$ data shown at 2 standard deviations, based on external precision. Multiple Res. = well producing from multiple reservoirs.

through diagenesis (Sivalingam, 1990). Thus, formation waters impacted by these mechanisms should show evidence for water–rock interactions related to smectite to illite conversion, namely depletion of K and preferential removal of ^{10}B, particularly in the more illite and chlorite-rich Wolfcamp shale (Schmidt, 1973; Williams et al., 2001a). Comparison of geometric centers between the shale and corresponding non-shale reservoirs (Table 1) and B composition and isotopic data (Fig. 8) show no evidence for either K or B loss (including preferential ^{10}B loss) in the water. Formation waters in the Wolfcamp and "Cline" shales thus appear to have entered these units after clay diagenesis was complete (Fig. 3). Processes other than clay diagenesis (discussed in the next section) were responsible for reducing salinity and changing the solute composition in the shale relative to water in the adjacent units.

Table 4
Sequential binary partition for the subcomposition [^{11}B, ^{10}B, Cl], where + indicates that part is in the numerator of the ilr balance, − indicates that the part is in the denominator of the ilr balance, r is the number of parts in the numerator, and s is the number of parts in the denominator. Parts with neither − or + are not used in that balance.

Partition	^{11}B	^{10}B	Cl	r	s
1	+1	+1	−1	2	1
2	+1	−1		1	1

4.3. Origin of formation waters in the Permian Basin

As described above, Na–Cl–Br plots help delineate the source of salinity in produced waters, but appear to be of limited help in understanding the origin of formation waters in the Permian Basin due to inputs of kerogen-derived halogens (particularly Br) and evidence from previous studies of recycling of halite near the basin margins of the hydrologically connected Palo Duro Basin (Hovorka et al., 1993; Knauth and Beeunas, 1986). Better evidence for origin of the brines can be yielded from δ^2H and $\delta^{18}O$ data (Dutton, 1987; Holser, 1979; Kharaka et al., 1987; Rowan et al., 2015), while insight into solute source is provided by $\delta^{11}B$ and $^{87}Sr/^{86}Sr$ data (Barnaby et al., 2004; Chapman et al., 2012; Moldovanyi et al., 1993; Williams et al., 2001b). Data for the elemental isotopes of water (Fig. 9) plot in proximity to the modern local meteoric water line (LMWL) of Reyes (2014), and the extent of data for primary and secondary fluid inclusions found in halite from the Palo Duro Basin (Knauth and Beeunas, 1986). Data for produced water samples from both the youngest (Guadalupian) and oldest (Devonian and Silurian) reservoirs plot near the modern local meteoric water line, suggesting that waters from these reservoirs are at least in part meteoric (Fig. 9). Samples from the same reservoirs host the lowest TDS concentrations, indicating meteoric contributions are an important source of lower salinity waters in the basin. Salinity data for formation waters for the Devonian-age reservoirs appear bi-modal, indicating that a potential vertical flow barrier may be present. Samples used here, from Devonian reservoirs, plot near the modern LMWL and exhibit TDS concentrations <50 g/L confirming the likely source of the lower salinity water in these units. Previous authors have suggested that the Late Devonian Woodford Shale represents a vertical flow barrier in the system (Merrill et al., 2015), but the location of the study samples relative to the Woodford is unknown for confirmation of this hypothesis. It is

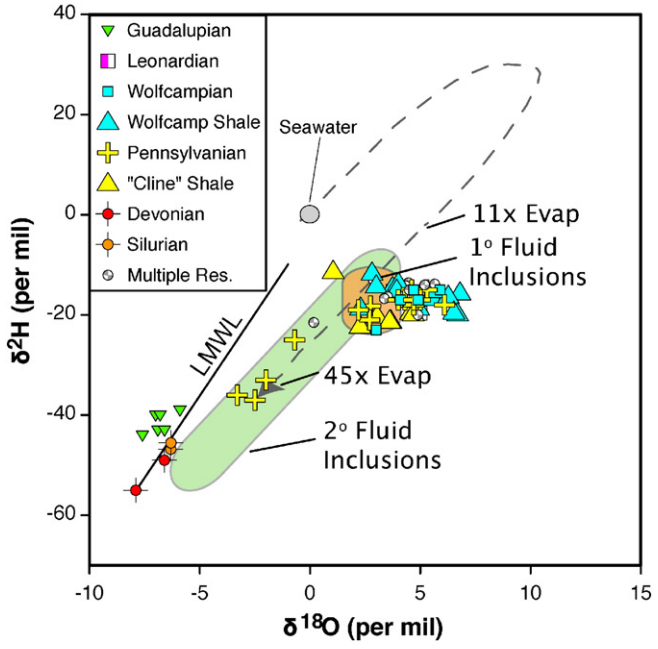

Fig. 9. Scatterplots of $\delta^{18}O$ and $\delta^{2}H$ data for produced water samples. Modern local meteoric water line (LMWL) from Reyes (2014). Also shown are the composition of seawater, the seawater evaporation trajectory of Holser (1979), and the composition of water in primary and secondary halite fluid inclusions from the Palo Duro Basin (Knauth and Beeunas, 1986). Multiple Res. = well producing from multiple reservoirs.

important to note that although the samples from Silurian reservoirs were collected distal to those from the Devonian reservoirs (Fig. 1), they still appear to be quite similar and follow TDS trends from the larger sample set indicating that patterns in the isotopic data are not likely controlled by local processes.

The remaining $\delta^{2}H$ and $\delta^{18}O$ data plot near the pathway for seawater evaporation (Holser, 1979), with the vast majority overlapping the range of data for primary fluid inclusions found within halite in the Palo Duro Basin, which are thought to represent evaporated Late Permian seawater (Knauth and Beeunas, 1986). A few of the data for samples from Pennsylvanian-aged reservoirs plot in the range of data for secondary fluid inclusions, which were interpreted to represent recycling of halite in the basin margins during inputs of continentally-derived freshwater into the system (Hovorka et al., 1993; Knauth and Beeunas, 1986). Such findings suggest that the majority of formation waters in Leonardian to Pennsylvanian-aged reservoirs consist of evaporated Late Permian seawater, which is related to the upper (Ochoan) Permian evaporites. Note that at the point of halite precipitation, geochemical modeling indicates that the estimated salinity of Late Permian seawater was 311,000 mg/L (Engle and Blondes, 2014). This value is far in excess of TDS concentrations measured in most of the samples from Guadalupian to Devonian reservoirs (Fig. 7), even though it roughly matches the $\delta^{2}H$ and $\delta^{18}O$ compositions of these samples. Dilution of the evaporated seawater by fresh meteoric water could have occurred but would have pushed the isotopic composition of the water off of the seawater evaporation pathway toward to the meteoric water line. A mixture of 60% Late Permian evaporated seawater concentrated by a factor of 4 times and 40% Late Permian evaporated seawater concentrated by a factor of 45 times produces roughly the same isotopic composition of water evaporated beyond the point of halite precipitation but with a much lower salinity (222,000 mg/L). This suggests that the observed composition of $\delta^{2}H$ and $\delta^{18}O$ and salinity of the samples represent a fairly homogeneous mixture of Late Permian seawater from different stages of evaporation, in agreement with models which call for cyclicity in the formation of evaporite deposits (Chaudhuri and Clauer, 1992).

Many of the data which plot near the composition of Late Permian seawater exhibit higher $\delta^{18}O$ values than the range of the fluid inclusion data. These same formation water samples show good agreement between their $\delta^{18}O$ values and those predicted assuming isotopic equilibrium with Wolfcampian and Pennsylvanian-age limestones in the basin (25.8–28.8‰ — Vienna Standard Mean Ocean Water basis; Saller et al., 1994) using fractionation factors based on estimated reservoir temperatures (Fig. 10). The similarity between $\delta^{2}H$ and $\delta^{18}O$ data for produced water samples from the "Cline" and Wolfcamp shales with those from the adjacent reservoirs also suggests that no additional source of meteoric or clay dehydration water has been added to the system, subsequently diluting the waters in the shales. Data for samples that plot outside the extent of primary fluid inclusions in Fig. 9, particularly from Guadalupian, Pennsylvanian (those that plot in the field for secondary fluid inclusions), Silurian, and Ordovician reservoirs also plot away from the trend predicted for oxygen exchange with carbonate minerals. This suggests that for these samples isotopic water–rock exchange with Paleozoic carbonate minerals is negligible.

Evidence for mixing and the origin of the fluids can be further enhanced using $^{87}Sr/^{86}Sr$ data in the produced waters and potential mineral sources of Sr. For minerals which contain abundant K (polyhalite and clays), previously developed Rb–Sr isochrons (Register and Brookins, 1980) were used to calculate the composition of these minerals during the Late Permian (252 Ma), when at least some of the fluids are thought to have formed. Nearly all of the data for samples with a suggested evaporated paleoseawater origin (Leonardian to Pennsylvanian) from the $\delta^{2}H$ and $\delta^{18}O$ results exhibit a narrow range of $^{87}Sr/^{86}Sr$ values (0.7085 to 0.7095), suggesting a common source. Conversely, samples which appear to be meteoric based on $\delta^{2}H$ and $\delta^{18}O$ results exhibit different, non-overlapping values, depending on the age of the reservoir. Such results support the hypothesis of different water sources for the fluids in

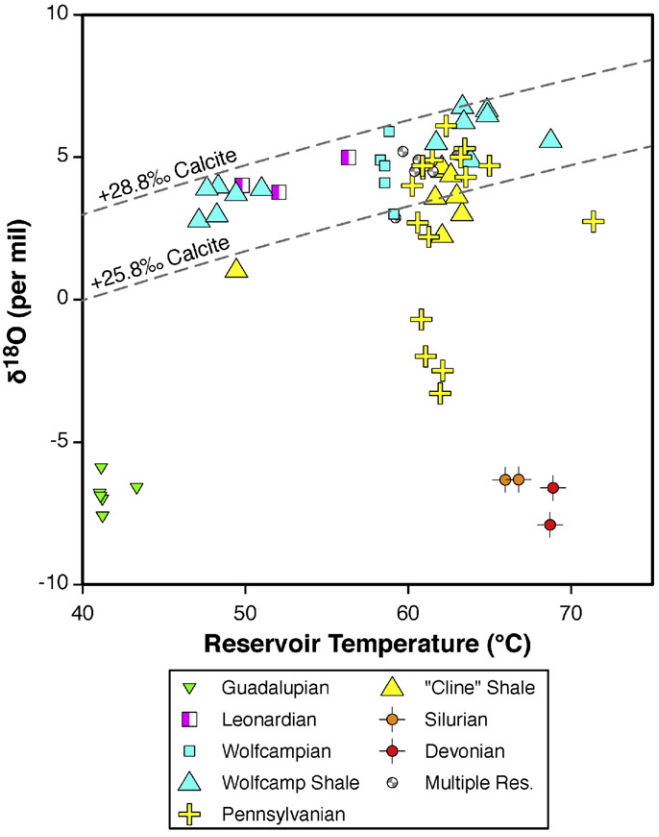

Fig. 10. Scatterplot of $\delta^{18}O$ versus estimated reservoir temperature showing the range of $\delta^{18}O$ values in isotopic equilibrium with Pennsylvanian and Wolfcampian age carbonates. Reservoir temperatures estimated using relationships between depth and corrected bottom hole temperatures in the study area using data from the Southern Methodist University National Geothermal Data System. Multiple Res. = well producing from multiple reservoirs.

Leonardian versus Devonian versus Silurian reservoirs despite all appearing to be meteoric-sourced. Based on a subset of the data presented here, Stueber et al. (1998) suggested a mixing trend between waters in the Devonian reservoirs and those in the Pennsylvanian reservoirs (Fig. 11). The linear trend on this $^{87}Sr/^{86}Sr$ versus 1/Sr plot is suggestive, but needs to be taken with caution given the limited dataset. However, this mixing would help to explain why some of the data for samples from Pennsylvanian reservoirs do not follow the predicted $\delta^{18}O$ values from isotopic exchange with Wolfcampian and Pennsylvanian limestones (Fig. 10). As an aside, use of 1/Sr concentration is not technically correct for CoDa (Blondes et al., 2015) but is still useful in identifying mixing, as it is linear in this space (mixing is non-linear in ilr transformed space).

Comparison of $^{87}Sr/^{86}Sr$ values from formation water samples with potential mineral samples in Ochoan and Guadalupian rocks (Hovorka et al., 1993; Register and Brookins, 1980) suggests that waters found in the Leonardian to Pennsylvanian reservoirs is the source of the Ochoan halite deposits across the Permian and Palo Duro Basins. This interpretation agrees with overlap of the $\delta^{18}O$ and $\delta^{2}H$ data for the same produced water samples with fluid inclusions in halite from the Palo Duro Basin (Fig. 9). The range of $^{87}Sr/^{86}Sr$ values for these formation waters and the halite + polyhalite samples (0.7085–0.7095) is far outside that of the Guadalupian anhydrite and limpid dolomite samples and of Mid- to Late-Permian seawater (0.7069–0.7076) described in the literature (Burke et al., 1982). Because there is little variance in the $^{87}Sr/^{86}Sr$ values in produced water samples from the Leonardian to Pennsylvanian reservoirs, the strontium signatures likely correspond to that of the evaporated paleoseawater when it began to sink into the basin, rather than post-infiltration water–rock reactions. One possible explanation for the radiogenic signature of the seawater in the basin during the Late Permian is that as progressive evaporation within the Permian Basin increased, moving from the Guadalupian into Ochoan Series (and thus moving from carbonate and anhydrite lithologies into halite), water flow from the west became increasingly restricted. In this scenario, radiogenic local dust inputs and sediment from arid river systems (Chaudhuri and Clauer, 1992; Register and Brookins, 1980) modified the $^{87}Sr/^{86}Sr$ values of the halite + polyhalite deposits outside of the range of bulk seawater during that period. Examination of the data for samples from Guadalupian reservoirs (which plot on the meteoric water line; Fig. 9) shows strong overlap with the Sr-bearing minerals in these units, supporting the idea that these waters have entrained most of their Sr from dissolution of these sequences. Lastly, the samples from Devonian and Silurian reservoirs (which plot on the meteoric water line; Fig. 9) show no common overlap with any of the evaporite minerals that cap the basin, suggesting that they may have been present prior to the Late Permian (Fig. 3).

Similar results are observed from the B isotopic data (Fig. 8). Formation waters from the Wolfcamp shale and Leonardian reservoirs fall in the range of predicted composition of Late Permian seawater evaporated beyond halite precipitation, although the former are slightly heavier than the latter (41.9–45.4‰ and 37.2–41.9‰, respectively). As previously discussed, waters in the "Cline" shale show additional enrichment of isotopically light B, likely derived from decomposition of marine kerogen in the shale. However, the two samples from Silurian reservoirs are distinct, exhibiting much lower $\delta^{11}B$ values of roughly 26‰. Although B isotopic data are not available for the reservoir rocks, at a reservoir temperature of 65 °C the isotopic separation (Δ) between silicate minerals and water is approximately −28‰, (Williams et al., 2001a). The corresponding $\delta^{11}B$ composition of sediments in equilibrium with these waters is roughly −2‰, which is close to the range of ancient marine sediments of −17.0 to −5.6‰ (Ishikawa and Nakamura, 1993).

Given a common origin of evaporated Late Permian seawater for brines from Leonardian to Upper Devonian reservoirs (mixture of pre- and post-halite saturation waters), processes which generated the lower salinity and high relative alkali content of formation waters from the Wolfcamp and "Cline" shale reservoirs are not obvious. Formation waters currently found in the shales likely entered after smectite to illite conversion (Fig. 3), so mechanisms other than clay diagenesis appear to be responsible. Clays act as semi-permeable membranes which limit movement of ions, particularly in the diffuse double layer near the clay–pore water interface (Magara, 1974), so diffusion of water into clay serves as one mechanism to lower salinity in formation water from shales in the Permian Basin. Laboratory and theoretical data show that for diffusion of seawater into clay, diffusion coefficients of multivalent ions are lower than those for univalent ions (Li and Gregory, 1974). Although the concentration gradient for each constituent, between the saline water in the carbonates and the less saline water originally present in the shales in the Permian Basin, is unknown, the differences between the effective diffusion coefficients for different compounds can be used to infer relative rates of diffusion. Thus,

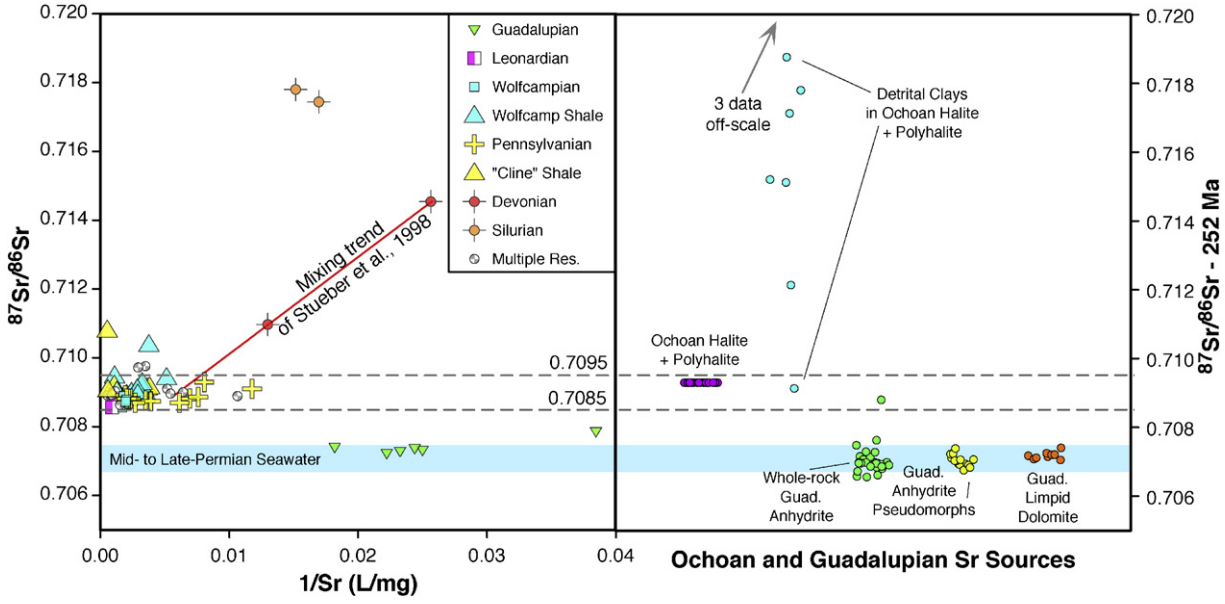

Fig. 11. Strontium isotopic data for formation water samples (left) and Ochoan and Guadalupian mineral sources (right). Random scatter along the x-axis applied to the mineral source data for each category to prevent overlapping of symbols. Data for mineral sources taken from Register and Brookins (1980) and Hovorka et al. (1993). Strontium isotopic data for Rb-bearing minerals (halite + polyhalite and detrital clays) corrected to their values during the Late Permian using the published Rb–Sr isochrons for the same samples. Estimated composition of Mid- to Late-Permian seawater taken from Burke et al. (1982). Multiple Res. = well producing from multiple reservoirs.

diffusion of solutes and water into shale reservoirs from sinking Late Permian seawater at near hydrostatic pressures (partially driven by an osmotic pressure gradient) might control shale formation water chemistry. Note, this mechanism is distinct from hyperfiltration mechanisms, which involves forcing water through clays under exceptionally high pressures. Theoretical calculations for diffusion of solutes into the Collovo-Oxfordian shale of the Paris Basin, a unit with a similar mineralogy to the Wolfcamp shale, show that effective diffusion coefficients for monovalent cations exceed those of divalent cations by up to a factor of three (Appelo et al., 2008). This limit is consistent with the results from the Permian Basin; the Na:Ca mass ratio for the geometric centers of produced waters from the Wolfcamp shale are 3.2 times higher than non-shale Wolfcampian reservoirs and the same ratio for the geometric centers for the "Cline" shale are 2.4 times higher than non-shale Pennsylvanian reservoirs. Moreover, Ca for Na ion exchange can also further increase Na/Ca ratios in clay minerals. This interpretation is also consistent with the limited boron isotope data. Although no studies on B isotope fractionation during diffusion into clays are known to exist, anions are retarded relative to neutral species in clays due to anion exclusion in the diffuse double layer (Magara, 1974). Given the affinity for ^{10}B in the borate anion, diffusion of boron would likely allow for faster transport of uncharged, ^{11}B-rich boric acid into clays producing an isotopically heavy pore water. This process might explain why $\delta^{11}B$ values for Wolfcamp shale formation water samples are slightly higher than those for Leonardian reservoirs (Fig. 8). Thus, we argue that the produced waters in the Wolfcamp and "Cline" shales are of the same origin as other fluids from Leonardian to Devonian reservoirs (evaporated Late Permian seawater), that diffused into the shales post-illitization (Fig. 3), leading to lower salinity water enriched in alkalis.

Despite low salinity fluids within the shales, salinity tends to increase with depth into Devonian reservoirs. This suggests that the dense, Late Permian seawater that sank into these deeper reservoirs, displacing less dense water previously present, was able to circumvent the low-permeability shales at the center of the basin. Large vertical structures to allow such deep fluid flow are generally absent in the basin. Platform and slope carbonates found around the basin margins (Hamlin and Baumgardner, 2012) are much more likely pathways for downward flow, allowing sinking brines to circumvent the basin-centered mudrock facies (Senger and Fogg, 1987).

Combining the various results (see Fig. 3 for summary of timing), meteoric waters found at the top and bottom of Paleozoic stratigraphic sections are separated by a nearly 1500–3000 m thick section of rock containing relatively homogenous (isotopically) Late-Permian seawater, which was mixed after evaporating to various degrees, to provide a composition with a salinity below that expected to produce halite, but with δ^2H and $\delta^{18}O$ signatures that suggest evaporation beyond halite formation. Such exceptionally dense fluids likely sunk into the basin, reacting with limestones in the Pennsylvanian and Wolfcampian reservoirs to produce the observed $\delta^{18}O$ values in some samples, at near-present reservoir temperatures. The source of meteoric water in lower salinity samples from Devonian to Ordovician rocks is unknown, although such units are part of the original Tobosa Basin, and extend for hundreds of kilometers. Pervasive karst and collapse features are found in equivalently aged Ordovician and Silurian units which outcrop near El Paso, Texas (Bellian et al., 2012), suggesting that a potential network for deep water storage and transport may exist beneath the Permian Basin. The source of the meteoric waters in the Guadalupian reservoirs is primarily thought to be derived from meteoric recharge to the west, where such units do or previously have outcropped (Barnaby et al., 2004; Bein and Dutton, 1993; Stueber et al., 1998).

4.4. Hydraulic connectivity between oil and gas reservoirs in the basin

Histograms of TDS concentrations and interpretations of isotopic data support the notion of intrusion of relatively fresh meteoric water, which gained salinity from the dissolution of evaporite minerals (Barnaby et al., 2004; Engle and Blondes, 2014; Lambert, 1992; Siegel and Anderholm, 1994) into Guadalupian and possibly Leonardian reservoirs. The bi-modal salinity of waters from Devonian reservoirs, and relatively low salinity of waters from Silurian and Ordovician reservoirs (<150 g/L) and meteoric source for those waters suggests another relatively distinct pocket of meteoric water, likely below the Woodford Shale. This deeper, chemically and isotopically distinct meteoric water is markedly different from the Late Permian seawater in overlying reservoirs, suggesting minimal communication between the two.

Histograms of in-situ pressure data from the three-county study area (Fig. 12) show differences in pressure gradients between the various reservoirs. Both Guadalupian and Leonardian reservoirs show modes (i.e., the interval with the highest frequency) that are slightly under-pressured (Fig. 12). Although some of this pattern may be related to fluid withdrawals during hydrocarbon production, under-pressuring was noted very early in the development of these fields (Elkins, 1953). Conversely, data from the Wolfcamp shale show substantial over-pressuring, consistent with its role as a source rock. Assuming maximum burial during the Eocene (Sinclair, 2007), fluid movement out of the Wolfcamp shale has been slow enough to retain some level of over-pressuring for at least 55 Ma, while allowing for under-pressuring to develop in Guadalupian and Leonardian reservoirs. Similarly, slight under-pressuring is also observed in Ordovician reservoirs, suggesting that downward fluid migration from the Wolfcamp shale and other over-pressured source rocks, has been limited (Fig. 12). Based on distinct chemical and pressure gradient differences between Late Permian seawater in Leonardian to Devonian reservoirs and meteoric waters found in older Paleozoic reservoirs, we suggest that the previously defined Deep Basin Brine Aquifer Systems of Bassett and Bentley (1982), be split into the overlying Deep Basin Brine Aquifer System and the underlying Deep Basin Meteoric Aquifer System (Fig. 2). We suggest the name for the latter to avoid confusion with paleo-meteoric water found in the Dockum and shallower portions of the basin and indicate proximity to the evaporated paleoseawater found above it.

Given a geologic history of uplift and tilting during the Laramide Orogeny and Basin and Range extension (Fig. 3), under-pressuring may have developed in more permeable layers, where eastward and southeastern flow exceeded recharge (Senger et al., 1987). In the case of Guadalupian and Leonardian reservoirs of the Permian Basin, some previous studies suggest that meteoric recharge to these reservoirs has occurred in and around the Guadalupe Mountains (Figs. 1, 4) and may be the source of meteoric waters in the same aquifers found further east into the Basin (Barnaby et al., 2004; Bein and Dutton, 1993; Stueber et al., 1998). However, more recent work in the Delaware Basin and Central Basin Platform suggests that encroachment of meteoric waters from the west is less spatially extensive in Guadalupian and Leonardian reservoirs than previously thought (Engle and Blondes, 2014). Hydrogeologic modeling of the Palo Duro Basin (Senger and Fogg, 1987) suggests that inputs from the meteoric waters sourced in New Mexico are limited in their range and that the majority of water which flow into Guadalupian and Leonardian units is through the relatively impermeable but expansive evaporite sequences. This conceptual model is also consistent with the rather uniform influx of meteoric waters across the entire basin, rather than being limited to the basin margins, and from observations of halite dissolution in several areas (Hovorka, 1998).

Within the Permian Basin, potential for upward fluid migration through natural conduits related to hydraulic fracturing of the Wolfcamp and "Cline" shales is minimal. Despite substantial over-pressuring in tight oil reservoirs, large-scale under-pressuring in Guadalupian reservoirs would greatly limit the potential for upward flow into shallower units, including drinking water reservoirs. In addition, fluid migration away from a fractured well is limited to the relatively short period between when the well is fractured (which is completed at pressures far exceeding reservoir pressures) and when the well goes into production (well pressure is set below reservoir pressure). However, this does not necessarily apply to potential transport of

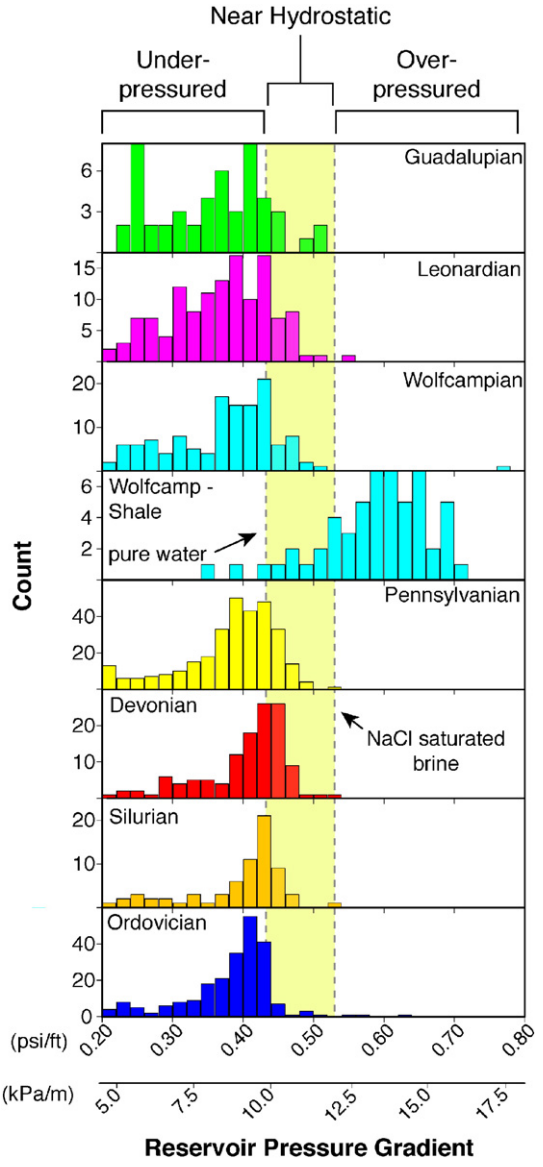

Fig. 12. Histograms showing reservoir shut-in pressure gradients from hydrocarbon reservoirs in Upton, Reagan, and Irion counties, Texas (Fig. 1).
Data taken from IHS Energy except for those for the Wolfcamp shale and a portion of the Leonardian reservoirs (Friedrich and Monson, 2013).

gas and water up well annuli, improperly abandoned wells, and other failures of infrastructure (Soeder et al., 2014; Vengosh et al., 2014).

5. Conclusions

Findings from this research examining formation waters in the eastern half of the Permian Basin suggest that during the Late Permian (Guadalupian into Ochoan), influx and mixing of evaporated seawater led to the creation of a fairly homogenous, dense volume of water, which is the original source of the evaporite minerals at the top of the Paleozoic sequence. These dense bitterns sunk down into underlying reservoirs, displacing the pre-existing fluids. The brines appear to have followed flow paths through the carbonate platforms on the basin margins, filling in permeable units around less-permeable shales and mudrocks, but were stopped above the Woodford Shale or other Devonian-age aquitards. Sulfate reduction appears to have greatly increased Ca/SO_4 ratios in these brines, and thus is partially responsible for their Ca–Cl-type composition. Sometime after smectite to illite conversion, diffusion of the paleoseawater into shales, such as the "Cline" and Wolfcamp, produced water that is isotopically indistinguishable from the source (O, H, and Sr isotopes) but has markedly lower salinity and is enriched in alkalis relative to alkaline earth elements. Release of NH_4, Br, I, and isotopically light B from marine kerogen in the "Cline" shale further modified the composition of the associated formation water. In deeper reservoirs (below the Woodford Shale), relatively old meteoric water was isolated from the overlying paleoseawater. We suggest that these two separate hydrogeologic units (previously referred to as a single hydrogeologic unit: the Deep Basin Brine Aquifer System) be split into the Deep Basin Brine Aquifer System and the underlying Deep Basin Meteoric Aquifer System, with the Woodford Shale acting as the assumed aquitard between them.

Uplift and tilting during the Laramide Orogeny and Basin and Range extension, allowed for eastward flow of formation waters in high permeability reservoirs and the development of associated underpressuring. This led to an influx of meteoric water possibly from uplifted areas in New Mexico, but also through the expansive and low-permeability evaporites which currently cap the Paleozoic sequence. Meteoric waters, reacting with the evaporites, produce a geochemically distinct brine in Guadalupian and some of the Leonardian reservoirs. As late as the Eocene, hydrocarbons reached maximum burial allowing for over-pressuring in the shales. This over-pressuring appears to be vertically limited in the current system, indicating that vertical fluid flow via natural conduits away from the shales is constrained and would likely be stopped at overlying and underlying under-pressured reservoirs. The lack of hydraulic communication between meteoric waters in Guadalupian reservoirs and the vestigial Late Permian seawater in the Wolfcamp and "Cline" shales indicates there is little chance for meteoric waters bringing in microbes to change the composition of the hydrocarbons in the source rocks, as has occurred in shallower units.

This effort shows that characterization of formation waters from shale reservoirs, particularly in comparison to those from non-shale units of similar age, is a beneficial tool for understanding paleofluid flow and origin within basins. Moreover, the examination of vertical salinity, chemical, isotopic, and pressure gradients are proxies for potential of fluid transport between reservoirs. Reservoir connectivity has implications for both environmental impacts of unconventional hydrocarbon production as well as understanding potential movement and influx of microbe-bearing meteoric water into source rocks. For these reasons, studying vertical fluid flow in brackish aquifers which overlie hydrocarbon reservoirs is an area of research which may yield more decisive information for upward fluid potential, to complement data generated from deeper basin brines. Given interest and concern over this topic, further research on vertical fluid flow in basins is an important priority.

Disclaimer

Use of trade, firm, or product names is for descriptive purposes only and does not imply endorsement by the U.S. Government.

Acknowledgments

Funding from this project was provided by the U.S. Geological Survey Energy Resources Program. The authors would like to thank Apache Corporation, CrownQuest, and Pioneer Natural Resources for access to sample their wells, valuable insight into their operations, and necessary data. Helpful conversations and feedback were provided by Elisabeth Rowan (USGS), Robert Baumgardner (Texas Bureau of Economic Geology), and Benjamin Brunner (UTEP). Assistance with fieldwork and laboratory analysis was provided by Madalyn Blondes (USGS), Tanya Gallegos (USGS), Belinda Gonzalez (UTEP), Josue Magana (NMSU), and Stephanie Ray (UTEP). Reviews by Gwen Macpherson (Univ. Kansas), Anna Martini (Amherst College), and Tina Roberts-Ashby (USGS) are acknowledged for providing critical and constructive feedback, which greatly improved the quality of this work.

Appendix A. Supplementary data

Chemical and isotopic data for the 39 samples collected as part of this investigation, including calculated values for molar log ratio used in Figs. 5, 6, and 8. Supplementary data associated with this article can be found in the online version, at http://dx.doi.org/10.1016/j.chemgeo.2016.01.025.

References

Appelo, C.A.J., Vinsot, A., Mettler, S., Wechner, S., 2008. Obtaining the porewater composition of a clay rock by modeling the in- and out-diffusion of anions and cations from an in-situ experiment. J. Contam. Hydrol. 101, 67–76. http://dx.doi.org/10.1016/j.jconhyd.2008.07.009.

Barnaby, R.J., Oetting, G.C., Gao, G., 2004. Strontium isotopic signatures of oil-field waters: applications for reservoir characterization. AAPG Bull. 88, 1677–1704.

Bassett, R.L., Bentley, M.E., 1982. Geochemistry and hydrodynamics of deep formation brines in the Palo Duro and Dalhart basins, Texas, U.S.A. J. Hydrol. 59, 331–372.

Bein, A., Dutton, A.R., 1993. Origin, distribution, and movement of brine in the Permian Basin (U.S.A.): a model for displacement of connate brine. Geol. Soc. Am. Bull. 1993, 695–707. http://dx.doi.org/10.1130/0016-7606(1993)105<0695:ODAMOB>2.3.CO;2.

Bellian, J.A., Kerans, C., Repetski, J.E., 2012. Digital outcrop model of stratigraphy and breccias of the southern Franklin Mountains, El Paso, Texas. In: Derby, J.D., Fritz, R.D., Longacre, S.A., Morgan, W.A., Sternbach, C.A. (Eds.), The Great American Carbonate Bank: the Geology and Economic Resources of the Cambrian–Ordovician Sauk Megasequence of Laurentia, pp. 909–939 http://dx.doi.org/10.1306/13331521M983516.

Bjølykke, K., 1998. Clay mineral diagenesis in sedimentary basins—a key to the prediction of rock properties. Examples from the North Sea Basin. Clay Miner. 33, 15–34. http://dx.doi.org/10.1180/000985598545390.

Blondes, M.S., Gans, K.D., Thordsen, J.J., Reidy, M.E., Thomas, B., Engle, M.A., Kharaka, Y.K., Rowan, E.L., 2014. U.S. Geological Survey National Produced Waters Geochemical Database, Version 2.1. http://eerscmap.usgs.gov/pwapp/.

Blondes, M.S., Engle, M.A., Geboy, N.J., 2015. Advances in integrating isotopic data with compositional data analysis: applications for deep formation brine geochemistry. In: Thió-Henestrosa, S., Martín-Fernández, J.A. (Eds.), Presented at the International Workshop on Compositional Data Analysis, Girona, Spain, p. 7.

Burke, W.H., Denison, R.E., Hetherington, E.A., Koepnick, R.B., Nelson, H.F., Otto, J.B., 1982. Variation of seawater $^{87}Sr/^{86}Sr$ throughout Phanerozoic time. Geology 10, 516–519. http://dx.doi.org/10.1130/0091-7613(1982)10<516:VOSSTP>2.0.CO;2.

Chapman, E.C., Capo, R.C., Stewart, B.W., Kirby, C.S., Hammack, R.W., Schroeder, K.T., Edenborn, H.M., 2012. Geochemical and strontium isotope characterization of produced waters from Marcellus Shale Natural Gas extraction. Environ. Sci. Technol. 46, 3545–3553. http://dx.doi.org/10.1021/es204005g.

Chaudhuri, S., Clauer, N., 1992. History of marine evaporites: constraints from radiogenic isotopes. In: Signatures, Isotopic, Records, Sedimentary (Eds.), Lecture Notes in Earth Sciences. Springer-Verlag, Berlin/Heidelberg, pp. 177–198 http://dx.doi.org/10.1007/BFb0009865.

Cortez, M., 2012. Chemostratigraphy, Paleoceanography, and Sequence Stratigraphy of the Pennsylvanian–Permian Section in the Midland Basin of West Texas With Focus on the Wolfcamp Formation (MS Thesis) University of Texas at Arlington, Arlington, Texas.

Dutton, A.R., 1987. Origin of brine in the San Andres Formation, evaporite confining system, Texas Panhandle and eastern New Mexico. Geol. Soc. Am. Bull. 99, 103–112.

Dutton, S.P., Kim, E.M., Broadhead, R.F., Raatz, W.D., Breton, C.L., Ruppel, S.C., Kerans, C., 2005. Play analysis and leading-edge oil-reservoir development methods in the Permian basin: increased recovery through advanced technologies. AAPG Bull. 89, 553–576. http://dx.doi.org/10.1306/12070404093.

Eastoe, C.J., Long, A., Knauth, L.P., 1999. Stable chlorine isotopes in the Palo Duro Basin, Texas: evidence for preservation of Permian evaporite brines. Geochim. Cosmochim. Acta 63, 1375–1382.

Egozcue, J.J., Pawlowsky-Glahn, V., 2005. Groups of parts and their balances in compositional data analysis. Math. Geol. 37, 795–828. http://dx.doi.org/10.1007/s11004-005-7381-9.

Elkins, L.F., 1953. Reservoir performance and well spacing, Spraberry Trend Area field of west Texas. Pet. Trans. 198, 177–196.

Engelhardt, W.V., Gaida, K.H., 1963. Concentration changes of pore solutions during the compaction of clay sediments. J. Sediment. Petrol. 33, 919–930.

Engle, M.A., Blondes, M.S., 2014. Linking compositional data analysis with thermodynamic geochemical modeling: oilfield brines from the Permian Basin, USA. J. Geochem. Explor. 141, 61–70. http://dx.doi.org/10.1016/j.gexplo.2014.02.025.

Engle, M.A., Rowan, E.L., 2013. Interpretation of Na–Cl–Br systematics in sedimentary basin brines: comparison of concentration, element ratio, and isometric log-ratio approaches. Math. Geosci. 45, 87–101. http://dx.doi.org/10.1007/s11004-012-9436-z.

Engle, M.A., Rowan, E.L., 2014. Geochemical evolution of produced waters from hydraulic fracturing of the Marcellus Shale, northern Appalachian Basin: a multivariate compositional data analysis approach. Int. J. Coal Geol. 126, 45–56.

Eppich, G.R., Wimpenny, J.B., Yin, Q.-Z., Esser, B.K., 2011. California GAMA special study: stable isotopic composition of boron in groundwater—analytical method development (No. Report LLNL-TR-498360). Lawrence Livermore National Laboratory.

Filzmoser, P., Hron, K., Reimann, C., 2009. Univariate statistical analysis of environmental (compositional) data: problems and possibilities. Sci. Total Environ. 407, 6100–6108. http://dx.doi.org/10.1016/j.scitotenv.2009.08.008.

Frenzel, H.N., Bloomer, R.R., Cline, R.B., Cys, J.M., Galley, J.E., 1988. The Permian basin region. In: Sloss, L.L. (Ed.), Sedimentary Cover — North American Craton. Geological Society of America, pp. 261–306.

Friedrich, M., Monson, G., 2013. Two practical methods to determine pore pressure regimes in the Spraberry and Wolfcamp Formations in the Midland Basin. Society of Petroleum Engineers Unconventional Resources Technology Conference Paper SPE-168834-MS, p. 12.

Galley, J.E., 1958. Oil and Geology in the Permian Basin of Texas and New Mexico: North America, In: Special Paper 18: Habitats of Oil. American Association of Petroleum Geology, pp. 395–446.

Hamlin, H.S., Baumgardner, R.W., 2012. Wolfberry (Wolfcampian-Leonardian) Deep-water Depositional Systems in the Midland Basin: Stratigraphy, Lithofacies, Reservoirs, and Source Rocks (No. Report of Investigations 277). Texas Bureau of Economic Geology.

Hansom, J., Lee, M.-K., 2005. Effects of hydrocarbon generation, basal heat flow and sediment compaction on overpressure development: a numerical study. Pet. Geosci. 11, 353–360. http://dx.doi.org/10.1144/1354-079304-651.

Herczeg, A.L., James Simpson, H., Anderson, R.F., Trier, R.M., Mathieu, G.G., Deck, B.L., 1988. Uranium and radium mobility in groundwaters and brines within the Delaware Basin, southeastern New Mexico, USA. Chem. Geol. 72, 181–196.

Holser, W.T., 1979. Trace elements and isotopes in evaporites. In: Burns, R.G. (Ed.), Marine Minerals. Mineralogical Society of America, Chelsea, Michigan, pp. 295–346.

Hounslow, A., 1995. Water Quality Data. Lewis Publishers, Boca Raton.

Hovorka, S.D., 1998. Characterization of Bedded Salt for Storage Caverns: Case Study From the Midland Basin (Open-file Report). Texas Bureau of Economic Geology.

Hovorka, S.D., Knauth, L.P., Fisher, R.S., Gao, G., 1993. Marine to nonmarine facies transition in Permian evaporites of the Palo Duro Basin, Texas: geochemical response. Geol. Soc. Am. Bull. 105, 1119–1134. http://dx.doi.org/10.1130/0016-7606(1993)105<1119:MTNFTI>2.3.CO;2.

Hunt, J.M., 1990. Generation and migration of petroleum from abnormally pressured fluid compartments. AAPG Bull. 74, 1–12.

Ishikawa, T., Nakamura, E., 1993. Boron isotope systematics of marine sediments. Earth Planet. Sci. Lett. 117, 567–580. http://dx.doi.org/10.1016/0012-821X(93)90103-G.

Joachimski, M.M., Simon, L., van Geldern, R., Lécuyer, C., 2005. Boron isotope geochemistry of Paleozoic brachiopod calcite: implications for a secular change in the boron isotope geochemistry of seawater over the Phanerozoic. Geochim. Cosmochim. Acta 69, 4035–4044. http://dx.doi.org/10.1016/j.gca.2004.11.017.

Khan, N.A., Engle, M., Dungan, B., Holguin, F.O., Xu, P., Carroll, K.C., 2016. Volatile-organic molecular characterization of shale-oil produced water from the Permian Basin. Chemosphere 148 (C), 126–136. http://dx.doi.org/10.1016/j.chemosphere.2015.12.116.

Kharaka, Y.K., Maest, A.S., Carothers, W.W., Law, L.M., Lamothe, P.J., Fries, T.L., 1987. Geochemistry of metal-rich brines from central Mississippi Salt Dome basin, U.S.A. Appl. Geochem. 2, 543–561.

Knauth, L.P., Beeunas, M.A., 1986. Isotope geochemistry of fluid inclusions in Permian halite with implications for the isotopic history of ocean water and the origin of saline formation waters. Geochim. Cosmochim. Acta 50, 419–433. http://dx.doi.org/10.1016/0016-7037(86)90195-X.

Konter, J.G., Storm, L.P., 2014. High precision $^{87}Sr/^{86}Sr$ measurements by MC-ICP-MS, simultaneously solving for Kr interferences and mass-based fractionation. Chem. Geol. 385, 26–34. http://dx.doi.org/10.1016/j.chemgeo.2014.07.009.

Lambert, S.J., 1992. Geochemistry of the waste isolation pilot plant (WIPP) site, southeastern New Mexico, USA. Appl. Geochem. 7, 513–531.

Li, Y.-H., Gregory, S., 1974. Diffusion of ions in sea water and in deep-sea sediments. Geochim. Cosmochim. Acta 38, 703–714.

Luo, M., Baker, M.R., LeMone, D.V., 1994. Distribution and generation of the overpressure system, Eastern Delaware Basin, Western Texas and Southern New Mexico. AAPG Bull. 78, 1386–1405.

Magara, K., 1974. Compaction, ion filtration, and osmosis in shale and their significance in primary migration. AAPG Bull. 58, 283–290.

Marcus, Y., 1989. Determination of pH in highly saline waters. Pure Appl. Chem. 61, 1133–1138.

Matchus, E.J., Jones, T.S., 1984. East–West Cross Section Through Permian Basin of West Texas. West Texas Geological Society.

McCaffrey, M.A., Lazar, B., Holland, H.D., 1987. The evaporation path of seawater and the coprecipitation of Br^- and K^+ with halite. J. Sed. Res. 57, 928–937.

Melzer, S., 2013. An Updated Assessment of the CO_2 Enhanced Oil Recovery Potential in the Vicinity of the Waste Isolation Pilot Plant. Melzer Consulting.

Merrill, M.K., Slucher, E.R., Roberts-Ashby, T.L., Warwick, P.D., Blondes, M.S., Freeman, P.A., Cahan, S.M., DeVera, C.A., Lohr, C.D., 2015. Geologic Framework for the National Assessment of Carbon Dioxide Storage Resources: Permian and Palo Duro Basins and Bend Arch–Fort Worth Basin. In: Warwick, P.D., Corum, M.D. (Eds.), Geologic Framework for the National Assessment of Carbon Dioxide Storage Resources, Open-file Report, p. 42 http://dx.doi.org/10.3133/ofr20121024K.

Miall, A.D., 2008. The southern midcontinent, Permian Basin, and Ouachitas. In: Miall, A.D. (Ed.), Sedimentary Basins of the World. Elsevier, pp. 297–327 http://dx.doi.org/10.1016/S1874-5997(08)00008-7.

Moldovanyi, E.P., Walter, L.M., Land, L.S., 1993. Strontium, boron, oxygen, and hydrogen isotope geochemistry of brines from basal strata of the Gulf Coast sedimentary basin, USA. Geochim. Cosmochim. Acta 57, 2083–2099.

Moran, J.E., 1996. Origin of iodine in the Anadarko Basin, Oklahoma: an ^{129}I study. AAPG Bull. 80, 685–693.

Nir, O., Marvin, E., Lahav, O., 2014. Accurate and self-consistent procedure for determining pH in seawater desalination brines and its manifestation in reverse osmosis modeling. Water Res. 64, 187–195. http://dx.doi.org/10.1016/j.watres.2014.07.006.

Pashin, J.C., McIntyre-Redden, M.R., Mann, S.D., Kopaska-Merkel, D.C., Varonka, M., Orem, W., 2014. Relationships between water and gas chemistry in mature coalbed methane reservoirs of the Black Warrior Basin. Int. J. Coal Geol. 126, 92–105.

Register, J.K., Brookins, D.G., 1980. Rb–Sr isochron age of evaporite minerals from the Salado formation (Late Permian), southeastern New Mexico: isochron. Isochron West 29, 39–42.
Reyes, F.R., 2014. Exploring the Hydrogeologic Controls on Brackish Water and Its Suitability for Use in Hydraulic Fracturing: the Dockum Aquifer, Midland Basin, Texas (MS Thesis) University of Texas at El Paso, El Paso, Texas.
Rosenbaum, M.S., 1976. Effect of compaction on the pore fluid chemistry of montmorillonite. Clay Clay Miner. 24, 118–121.
Rowan, E.L., Engle, M.A., Kraemer, T.F., Schroeder, K.T., Hammack, R.W., Doughten, M.W., 2015. Geochemical and isotopic evolution of water produced from Middle Devonian Marcellus shale gas wells, Appalachian basin, Pennsylvania. AAPG Bull. 99, 181–206.
Saller, A.H., Dickson, J., Boyd, S.A., 1994. Cycle stratigraphy and porosity in Pennsylvanian and Lower Permian shelf limestones, eastern Central Basin Platform, Texas. AAPG Bull. 78, 1820–1842.
Schmidt, G.W., 1973. Interstitial water composition and geochemistry of deep Gulf Coast shales and sandstones. AAPG Bull. 57, 321–337.
Senger, R.K., Fogg, G.E., 1987. Regional underpressuring in Deep Brine Aquifers, Palo Duro Basin, Texas: 1. Effects of hydrostratigraphy and topography. Water Resour. Res. 23, 1481–1493. http://dx.doi.org/10.1029/WR023i008p01481.
Senger, R.K., Kreitler, C.W., Fogg, G.E., 1987. Regional underpressuring in Deep Brine Aquifers, Palo Duro Basin, Texas: 2. The effect of Cenozoic basin development. Water Resour. Res. 23, 1494–1504. http://dx.doi.org/10.1029/WR023i008p01494.
Siegel, M.D., Anderholm, S., 1994. Geochemical evolution of groundwater in the Culebra dolomite near the Waste Isolation Pilot Plant, southeastern New Mexico, USA. Geochim. Cosmochim. Acta 58, 2299–2323.
Sinclair, T.D., 2007. The generation and continued existence of overpressure in the Delaware Basin, Texas (PhD thesis) Durham University, Durham, UK.
Sivalingam, S., 1990. Clay diagenesis of the source rocks from the Permian Basin \ Texas Tech University, Lubbock, Texas.
Soeder, D.J., Sharma, S., Pekney, N., Hopkinson, L., Dilmore, R., Kutchko, B., Stewart, B., Carter, K., Hakala, A., Capo, R., 2014. An approach for assessing engineering risk from shale gas wells in the United States. Int. J. Coal Geol. 126, 4–19.
Sofer, Z., Gat, J.R., 1972. Activities and concentrations of oxygen-18 in concentrated aqueous salt solutions: analytical and geophysical implications. Earth Planet. Sci. Lett. 15, 232–238. http://dx.doi.org/10.1016/0012-821X(72)90168-9.
Sofer, Z., Gat, J.R., 1975. The isotope composition of evaporating brines: effect of the isotopic activity ratio in saline solutions. Earth Planet. Sci. Lett. 26, 179–186.
Stein, C.L., Krumhansl, J.L., 1988. A model for the evolution of brines in salt from the lower Salado Formation, southeastern New Mexico. Geochim. Cosmochim. Acta 52, 1037–1046.
Stueber, A.M., Saller, A.H., Ishida, H., 1998. Origin, migration, and mixing of brines in the Permian Basin: geochemical evidence from the eastern Central Basin Platform, Texas. AAPG Bull. 82, 1652–1672.
Tolosana-Delgado, R., Otero, N., Soler, A., 2005. A compositional approach to stable isotope data analysis. Presented at the CoDaWork '05: 2nd International Conference on Compositional Data Analysis, pp. 1–11.
U.S. Energy Information Administration, 2016. Drilling productivity report. http://www.eia.gov/petroleum/drilling/ (Accessed: January 25, 2016).
Vengosh, A., Starinsky, A., Kolodny, Y., Chivas, A.R., Raab, M., 1992. Boron isotope variations during fractional evaporation of sea water: new constraints on the marine vs. nonmarine debate. Geology 20, 799–802.
Vengosh, A., Jackson, R.B., Warner, N., Darrah, T.H., Kondash, A.J., 2014. A critical review of the risks to water resources from unconventional shale gas development and hydraulic fracturing in the United States. Environ. Sci. Technol. http://dx.doi.org/10.1021/es405118y.
Vidic, R.D., Brantley, S.L., Vandenbossche, J.M., Yoxtheimer, D., Abad, J.D., 2013. Impact of shale gas development on regional water quality. Science 340, 1235009-1235009. http://dx.doi.org/10.1126/science.1235009.
Ward, R.F., Kendall, C.G.S.C., Harris, P.M., 1986. Upper Permian (Guadalupian) facies and their association with hydrocarbons–Permian basin, west Texas and New Mexico. AAPG Bull. 70, 239–262.
Walter, L.M., Stueber, A.M., Huston, T.J., 1990. Br-Cl-Na systematics in Illinois basin fluids: constraints on fluid origin and evolution. Geology 18, 315–318.
Williams, L.B., Hervig, R.L., Holloway, J.R., Hutcheon, I., 2001a. Boron isotope geochemistry during diagenesis. Part I. Experimental determination of fractionation during illitization of smectite. Geochim. Cosmochim. Acta 65, 1769–1782.
Williams, L.B., Hervig, R.L., Wieser, M.E., Hutcheon, I., 2001b. The influence of organic matter on the boron isotope geochemistry of the gulf coast sedimentary basin, USA. Chem. Geol. 174, 445–461.
Worden, R.H., 1996. Controls on halogen concentrations in sedimentary formation waters. Mineral. Mag. 60, 259–274.